Complex geometry and integrated macro-porosity: Clinical applications of electron beam melting to fabricate bespoke bone-anchored implants

Acta Biomaterialia 156 (2023) 125–145

Contents lists available at ScienceDirect

Acta Biomaterialia

journal homepage: www.elsevier.com/locate/actbio

Review article

Complex geometry and integrated macro-porosity: Clinical applications of electron beam melting to fabricate bespoke bone-anchored implants☆

Anders Palmquist[a,*], Martina Jolic[a], Eduard Hryha[b], Furqan A. Shah[a,*]

[a] Department of Biomaterials, Institute of Clinical Sciences, Sahlgrenska Academy, University of Gothenburg, Gothenburg, Sweden
[b] Department of Materials and Manufacturing Technologies, Chalmers University of Technology, Gothenburg, Sweden

ARTICLE INFO

Article history:
Received 15 February 2022
Revised 16 May 2022
Accepted 1 June 2022
Available online 5 June 2022

Keywords:
Electron beam melting
Additive manufacturing
Human
Bone
Implant
Biomaterials

ABSTRACT

The last decade has witnessed rapid advancements in manufacturing technologies for biomedical implants. Additive manufacturing (or 3D printing) has broken down major barriers in the way of producing complex 3D geometries. Electron beam melting (EBM) is one such 3D printing process applicable to metals and alloys. EBM offers build rates up to two orders of magnitude greater than comparable laser-based technologies and a high vacuum environment to prevent accumulation of trace elements. These features make EBM particularly advantageous for materials susceptible to spontaneous oxidation and nitrogen pick-up when exposed to air (e.g., titanium and titanium-based alloys). For skeletal reconstruction(s), anatomical mimickry and integrated macro-porous architecture to facilitate bone ingrowth are undoubtedly the key features of EBM manufactured implants. Using finite element modelling of physiological loading conditions, the design of a prosthesis may be further personalised. This review looks at the many unique clinical applications of EBM in skeletal repair and the ground-breaking innovations in prosthetic rehabilitation. From a simple acetabular cup to the fifth toe, from the hand-wrist complex to the shoulder, and from vertebral replacement to cranio-maxillofacial reconstruction, EBM has experienced it all. While sternocostal reconstructions might be rare, the repair of long bones using EBM manufactured implants is becoming exceedingly frequent. Despite the various merits, several challenges remain yet untackled. Nevertheless, with the capability to produce osseointegrating implants of any conceivable shape/size, and permissive of bone ingrowth and functional loading, EBM can pave the way for numerous fascinating and novel applications in skeletal repair, regeneration, and rehabilitation.

Statement of significance

Electron beam melting (EBM) offers unparalleled possibilities in producing contaminant-free, complex and intricate geometries from alloys of biomedical interest, including Ti6Al4V and CoCr. We review the diverse range of clinical applications of EBM in skeletal repair, both as mass produced off-the-shelf implants and personalised, patient-specific prostheses. From replacing large volumes of disease-affected bone to complex, multi-material reconstructions, almost every part of the human skeleton has been replaced with an EBM manufactured analog to achieve macroscopic anatomical-mimickry. However, various questions regarding long-term performance of patient-specific implants remain unaddressed. Directions for further development include designing personalised implants and prostheses based on simulated loading conditions and accounting for trabecular bone microstructure with respect to physiological factors such as patient's age and disease status.

☆ Part of the Special Issue on Biofabrication for Orthopedic, Maxillofacial, and Dental Applications, guest-edited by Professors Hala Zreiqat, Khoon Lim, and Debby Gawlitta

* Corresponding authors.
E-mail addresses: anders.palmquist@biomaterials.gu.se (A. Palmquist), furqan.ali.shah@biomaterials.gu.se (F.A. Shah).

https://doi.org/10.1016/j.actbio.2022.06.002
1742-7061/

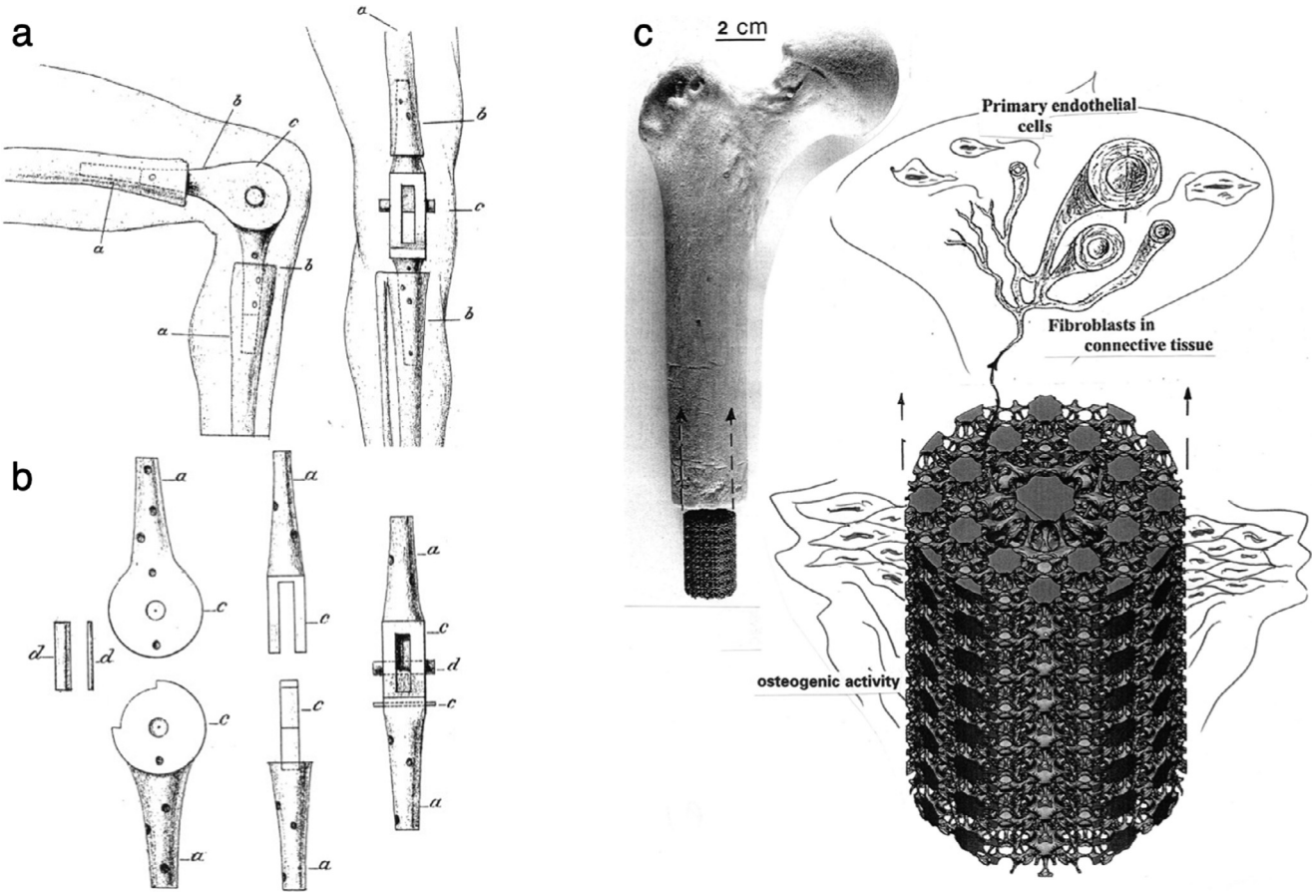

Fig. 1. (a–b) Gluck's hinged prosthetic knee implant. (a) Distal femoral and proximal tibial resections are made to expose the medullary canal, into which the cylindrical ends of the prosthesis are implanted. (b) Two implants made of ivory are connected to form a hinge. The proximal and distal portions are connected by a pin, which acts as the bearing, and thus allows for single-axis rotation about the pin. From Gluck T. 2011. Clin Orthop Relat Res. Adapted with permission from Wolters Kluwer Health, Inc. [3]. (c) The "living implant" concept. 3D printed femoral stem having a graded unit cell. Blood vessel development, osteoblast migration and growth in a connective matrix within the macro-porous structure. From Murr et al. 2017. J Mech Behav Biomed Mater. Adapted with permission from Elsevier [5].

1. Introduction

The use of prosthetic devices dates back thousands of years, from ancient mythology to the relatively recent Roman *Capua Leg* (circa 300 BC) made of bronze, which is one of the earliest known prosthetic limbs [1]. In modern times, total joint replacement with implanted devices has been recorded as early as the 1890s (Fig. 1a–b), with the pioneering work of Themistocles Gluck who used a hinge prosthesis made of ivory together with mixtures of rosin, pumice, and plaster as the *bone cement* in total knee replacement [2,3]. Biofabrication encompasses the production of complex living and non-living biological products (or systems) from living cells, molecules, extracellular matrices, and biomaterials [4]. The concept of a '*living implant*' has been presented by Lawrence Murr and colleagues (Fig. 1c), where blood vessels develop, and osteoblasts are able to migrate and grow in a connective matrix within the macro-porous structure of a 3D printed implant [5].

Metal implants have long been in clinical use, for restoring lost function, replacing missing body parts, and anchoring prosthetic devices. Although commercially pure titanium (cp-Ti) and titanium alloy (typically, Ti6Al4V) predominate [6] in dentistry and orthopaedics, various other metals and alloys (including cobalt chromium, stainless steel, tantalum, and magnesium) are in use for different applications. The surface properties of dental implants play important roles in modulating the cellular and molecular interactions between the implant surface and the surrounding tissues, and eventual bone regeneration [7]. Various procedures are used to modify the surface physico-chemical properties of dental implants [8]. In orthopaedics, although the replacement of a diseased or dysfunctional hip started with excision of the femoral head in the 18th and 19th century, successful total hip replacement with metallic implants, of which the Charnley hip and the Exeter hip are important examples, was not achieved until the late 20th century [9]. Currently, total hip replacement is one of the most common surgical procedures performed [10], and it is estimated that about three quarters of hip replacements last for ~15–20 years. [11]. A major challenge associated with metal implants is that of stress shielding caused by the stiffness mismatch between the implant and the surrounding bone [12]. Young's moduli of cortical bone and trabecular bone are ~3–30 GPa and ~0.02–2 GPa, respectively. In comparison, Young's moduli of Ti6Al4V (ASTM F136) and CoCr (ASTM F75) are ~110 GPa and ~210 GPa, respectively. Density optimisation at the bone-implant interface, such as by reducing the effective density (i.e., total porosity) and therefore the Young's modulus using additive manufacturing can minimise stress shielding [13]. And in this context, the potential for use of highly porous implants in total knee replacement was recognised very early (Fig. 2) [14].

2. Powder Bed Fusion based metal additive manufacturing

Powder Bed Fusion (PBF) techniques share the same basic principles of all additive manufacturing technologies, i.e., layer-by-

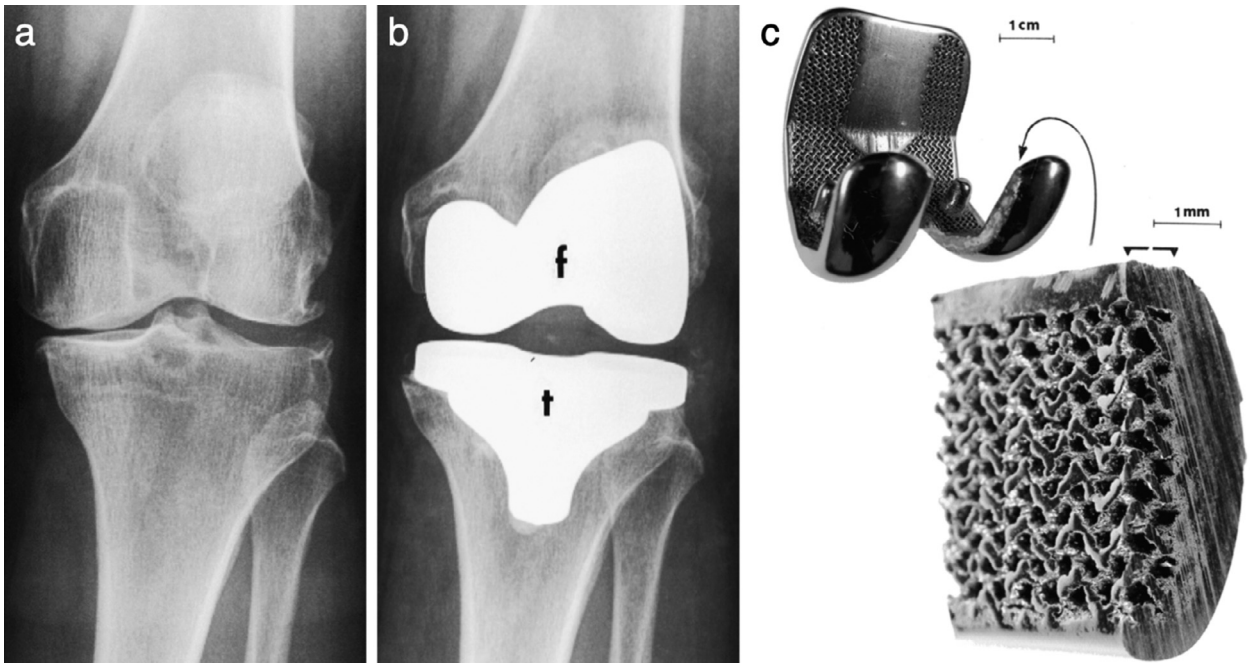

Fig. 2. (a–c) From conventional to additively manufactured components for total knee replacement. (a) Left knee before knee replacement. (b) Contemporary, commercial, orthopaedic total knee replacements consist of a CoCr femoral component, f, and a Ti6Al4V tibial component, t, cemented into place using acrylic cement. The CoCr component is cast while the Ti6Al4V component is usually fabricated from wrought stock. (c) CoCr alloy prototype corresponding to the femoral component made by electron beam melting (EBM), hot isostatic pressing (HIP) annealed, machined, and partially polished. From Murr et al. 2011. J Mech Behav Biomed Mater. Adapted with permission from Elsevier [14].

layer fabrication using data from a 3D model. Using a high-energy source, either a laser beam (PBF-LB) or an electron beam (PBF-EB), the powder in the powder bed is selectively melted – one layer at a time [15]. Utilisation of a high spatial resolution energy source in combination with fine powder feedstock allows production of geometrically complex components with fine features, e.g., 3D cellular structures with interconnected and/or graded porosity [16], suitable for bone ingrowth [17], and skeletal reconstruction [18]. PBF-EB is also referred to as electron beam melting (EBM). An electron beam (up to ~6 kW power) is generated from a tungsten filament or a lanthanum hexaboride (LaB6) cathode and is controlled by electromagnetic lenses that allow scanning the powder bed surface at speeds up to 10 km/s, resulting in build rates up to two orders of magnitude higher than PBF-LB [19]. However, use of an electron beam requires controlled vacuum at pressures below 10^{-6} bar in order to prevent collisions between electrons and air molecules. Processing in vacuum also has the advantage of minimising powder degradation by greatly reducing powder interaction with the residual air in the process chamber, which typically results in powder oxidation and nitrogen pick-up. This is especially critical in the case of materials with high activity, e.g., Ti and Ti6Al4V. Therefore, the use of standardised, high-purity powders [20,21] under vacuum processing during EBM allows control over accumulation of trace elements such as oxygen, that may impact the mechanical properties [22]. For example, the yield strength (~850 MPa), tensile strength (~950 MPa), and elongation to failure (~20%) of EBM manufactured Ti6Al4V after hot isostatic pressing are comparable to (or even better than) wrought and forged counterparts [19]. While the yield strength (~860–1000 MPa) and tensile strength (~930–1100 MPa) of PBF-LB manufactured Ti6Al4V are comparable to EBM manufactured Ti6Al4V, the elongation to failure is typically lower in comparison [23].

The first step during EBM processing is distribution of a thin layer (50–150 µm) of powder, using a flexible metal blade. Interaction of the electron beam with the powder may create electrostatic charging, resulting in sudden dispersion of charged particles (referred to as '*smoking*') [24]. Therefore, the entire surface of the powder bed is pre-sintered using a defocussed electron beam, which results in the formation of inter-particle necks and enables reaching the desired preheating temperature. With increasing particle size, the powder becomes more resistant to smoking [24]. The use of coarser particles (between 45 and 106 µm) compared to other powder-based, additive manufacturing technologies (e.g., PBF-LB or binder jetting) together with higher layer thickness results in higher surface roughness of EBM manufactured components ($R_a \approx$ 25–35 µm) [19,25]. Pre-sintering improves the electrical conductivity [26] and mechanical stability of the powder bed required for further selective melting of the deposited layer, resulting in formation of the final-shaped component inside a semi-sintered powder cake. Pre-sintering and pre-heating allow to minimise residual stresses in the as-fabricated components and reduce component distortion. At the same time, the pre-sintered cake possesses necessary mechanical strength providing full freedom when it comes to the nesting and stacking parts on top of each other, not possible with PBF-LB. This allows to maximise the use of the available build volume and hence results in further improved productivity of the EBM process. With the use of established process parameters, certain mechanical properties of EBM manufactured Ti6Al4V such as strength and elongation are comparable to (or even better than) wrought and forged counterparts [19]. On the other hand, the fatigue performance of EBM manufactured Ti6Al4V is typically inferior [27], but can be improved significantly by post treatments. Hot isostatic pressing reduces porosity [28], allows manipulation of microstructure to achieve equiaxed grains to ensure isotropic mechanical properties [29], and improve mechanical properties, including ductility (elongation to failure) and fatigue behaviour [30]. Subsequent surface treatments such as centrifugal finishing, linishing, shot peening, and laser shock peening can fur-

ther improve the fatigue strength [31]. Post-processing procedures are reported to increase the cost of the manufacturing by 4–13% [32].

The mechanical properties of EBM manufactured, open cellular constructs are strongly dependent on the lattice structure and the process parameters. These are typically determined using standard compressive tests, in accordance with ISO 13314, and typically exhibit a linear relationship with the relative density [5,13,14]. Pioneering preclinical studies have shown that EBM produced materials, with both as-produced surface and machined surface show similar (or at least comparable) osseointegrative properties for solid implants [33], potential for bone ingrowth in macro-porous implants [34–36], and good biocompatibility [37]. Moreover, *in vivo* studies demonstrate that Ti6Al4V and CoCr osseointegrate to comparable levels, especially in terms of molecular composition of peri-implant bone extracellular matrix [38]. Furthermore, as an indicator of bone-bonding ability of biomaterials, osteocytes have been shown to establish direct dendritic connectivity with both Ti6Al4V [38] and CoCr [39]. But despite concerns around toxicity of the various alloying elements that may be released, the biocompatibility is generally deemed acceptable for long term use, together with excellent resistance to corrosion and wear [40]. As such, both alloys have been in clinical use for several decades. Nevertheless, it remains to be seen if significant complications can be induced by particulate wear debris from EBM manufactured devices, which may be too large for macrophages to phagocytose and/or enzymatically degrade.

EBM manufactured macro-porous constructs have been used extensively in veterinary orthopaedic surgery. A notable example is the repair of cranial cruciate ligament rupture in dogs by tibial tuberosity advancement using porous EBM implants [41]. In clinical use, besides mass produced and standardised, *off-the-shelf* implants such as acetabular cups, fixations pins, scaphoid bone replacement, and hemipelvic implants, personalised, *patient-specific* implants have been produced for almost every part of the human skeleton.

3. Off-the-shelf implants

3.1. Acetabular cups

Acetabular cups used in total hip arthroplasty are among the earliest clinical applications of porous EBM produced implants, where implants with integrated porous networks are readily mass produced. Comparative analysis between retrieved EBM produced acetabular cups (Delta TT; LimaCorporate, Italy) and conventional acetabular cups produced by forging and milling (Pinnacle Porocoat; DePuy Synthes, USA) revealed expected differences attributable to implant manufacturing processes, i.e., a thicker porous layer, higher percentage porosity, and larger pore size of EBM manufactured acetabular cups (EBM cups, Fig. 3a) [42]. Histomorphometric analysis of EBM cups (Delta TT and Delta ONE, LimaCorporate, Italy) and conventional uncemented acetabular cups (Trident I Tritanium, Stryker, USA; R3 STIKTITE, Smith & Nephew, USA; Pinnacle Gription, DePuy Synthes, USA) provided further evidence in support of better bone ingrowth, including bone area (%) and bone-implant contact (%), for EBM cups [43]. Clinical data from different manufacturers suggests relatively low failure rates of EBM cups. Evidence from a large retrospective study involving over 9000 patients reveals a significantly lower rate of aseptic loosening for highly porous acetabular cups with an integrated porous network (Fixa Ti-Por, Adler Ortho, Italy), at 0.1%, compared to all other cementless acetabular cups, at 0.3% (Fig. 3b–d) [44]. Cementless EBM cups (3D ACT, AK Medical, China) characterised by a ~1.5 mm porous layer (600–800 μm pore size range, ~80% porosity) over a solid base have shown promising short-term results with no failures at 2 year follow-up in 92 consecutive patients [45]. A separate study using the same acetabular cups reports a survival rate of 96.3% at ~8 year follow-up (Fig. 3e) [46].

3.2. Hemipelvic implants

Several types of EBM manufactured pelvic endoprostheses are in clinical use. One study, investigating the performance of standard (one-piece, non-adjustable) hemipelvic prostheses, screw-rod connected (two-piece, adjustable) hemipelvic prostheses, and iliac prostheses reports an overall survival of 85%. Although one in five patients experienced delayed wound healing and two patients suffered hip dislocation, no deep infections, implant loosening, or displacement of the components was recorded [47]. In the pelvic area, tumour resections requiring larger reconstructions have been shown to benefit from 3D printed modular hemipelvic endoprostheses (GPS, AK Medical, China). Placed in 80 consecutive patients, the 3-year survival rate of such prostheses is 91.6%, where the main causes of implant failure/removal were infection or local tumour recurrence (Fig. 3f–i) [48].

3.3. Fixation pins for osteonecrotic femoral heads

In certain stages of osteonecrosis of the femoral head, early intervention can delay the need for total hip arthroplasty. An EBM, split-design fixation pin has been developed (Fig. 3j–k). A major advantage of the split-design is that the fixation pin can be removed from the femoral head if a total hip arthroplasty is eventually required. Hip preservation using a split-design fixation pin was more successful in patients at early-stage osteonecrosis, without obvious signs of infection or pin loosening at 24-month follow-up [49].

3.4. Metaphyseal components

Metaphyseal cones and sleeves for use in total knee replacement manufactured at ~60% porosity and 330–390 μm strut thickness (EPORE®, Implantcast GmbH, Germany) are designed to promote bone ingrowth and improve implant stability (Fig. 3i). According to a retrospective study involving 22 patients, postoperative infection occurred in two individuals, however, no early fixation failures were reported and radiographic signs of bone ingrowth were evident at the most recent follow-up (2–44 months) [50].

3.5. Wrist (scaphoid bone)

Approximately 5–10% of all scaphoid fractures end up in non-union, particularly if the bone fragments are displaced [51]. Such a scaphoid non-union with a necrotic area was successfully repaired with a partial scaphoid replacement using custom-made titanium implant. Implant design included a hole for scapholunate interosseous ligament reconstruction [52]. The same strategy has been implemented for total scaphoid replacement, following non-union and necrosis in both fragments (Fig. 3m–o) [53].

4. Personalised, patient-specific implants

4.1. Cranial

Large calvarial defects due to trauma or tumour resection have been successfully reconstructed using 2 mm thick, custom-made endoprostheses (Fig. 4a–b) [54]. A similar approach was taken in a larger study with comparable success. In a majority of cases, the primary reason behind the use of EBM manufactured constructs was failure of the initial reconstruction due to infection. Constructs

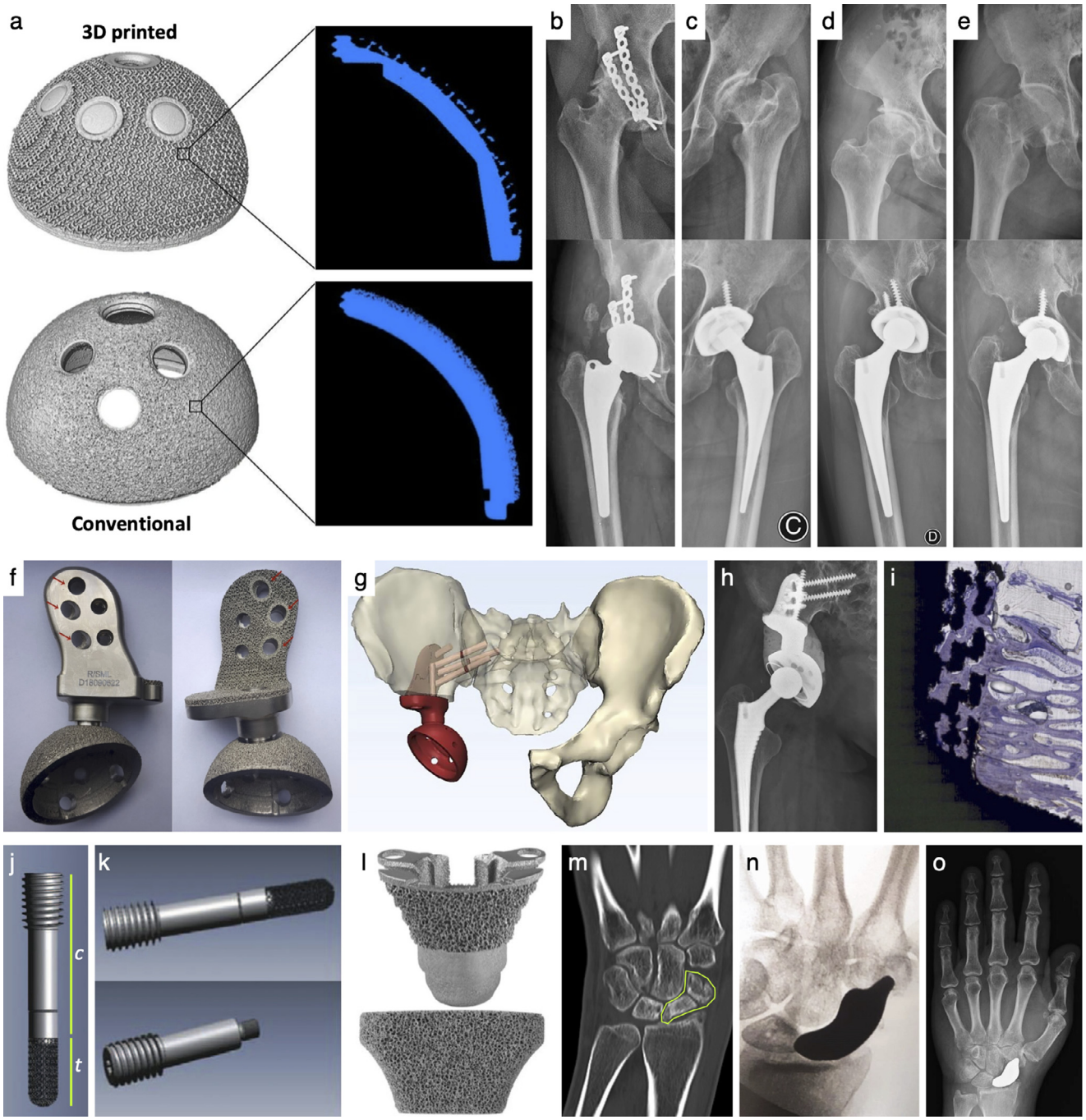

Fig. 3. (a) Comparison of 3D printed (Delta TT; LimaCorporate, Italy) and conventional (Pinnacle Porocoat; DePuy Synthes, USA) acetabular cups. X-ray micro-computed tomography reconstruction of the whole implant and a cross-section showing the porous structure. From Dall'Ava et al. 2020. J Orthop Surg Res. Reproduced under the terms of the CC BY 4.0 [42]. (b–e) 3D printed acetabular cup in total hip arthroplasty. (b) Osteoarthritic left hip with previous acetabular fracture (top) and 60-month postoperative (bottom). From Castagnini et al. 2019. Int Orthop. Adapted with permission from Springer Nature [44]. (c) Developmental dysplasia of the hip (top) and 90-month postoperative (bottom). (d) Femoral head necrosis (top) and 60-month postoperative (bottom). (e) Femoral neck fracture (top) and 63-month postoperative (bottom). From Huang et al. 2021. Orthop Surg. Reproduced under the terms of the CC BY 4.0 [46]. (f–i) Modular hemipelvic endoprosthesis. (f). 3D printed prosthesis. (g) Illustration of modular hemipelvic endoprosthesis with iliosacral fixation, where loading stresses from the trunk are balanced by supporting forces from the lower extremities. (h) Radiograph, 3 years after pelvic reconstruction. (i) Bone ingrowth into the porous structure. Histology. From Ji et al. 2020. J Bone Joint Surg Am. Adapted with permission from Wolters Kluwer Health, Inc. [48]. (j–k) Split-design fixation pin for the femoral head. (j) Trabecular portion, t, and connecting rod, c. (k) Split-design fixation pin shown with (top) and without (bottom) the trabecular portion. From Zhang et al. 2018. Medicine (Baltimore). Reproduced under the terms of the CC BY-ND 4.0 [49]. (l) Metaphyseal cone (left) and sleeve (right). From England et al. 2021. J Clin Orthop Trauma. Adapted with permission from Elsevier [50]. (m–o) Scaphoid non-union and necrosis. (m) Computed tomography, preoperative. (n) Intraoperative imaging to confirm positioning of the implant. (o) Radiograph, 12-months postoperatively. From Rossello MI. 2020. Case Reports Plast Surg Hand Surg. Reproduced under the terms of the CC BY 4.0 [53].

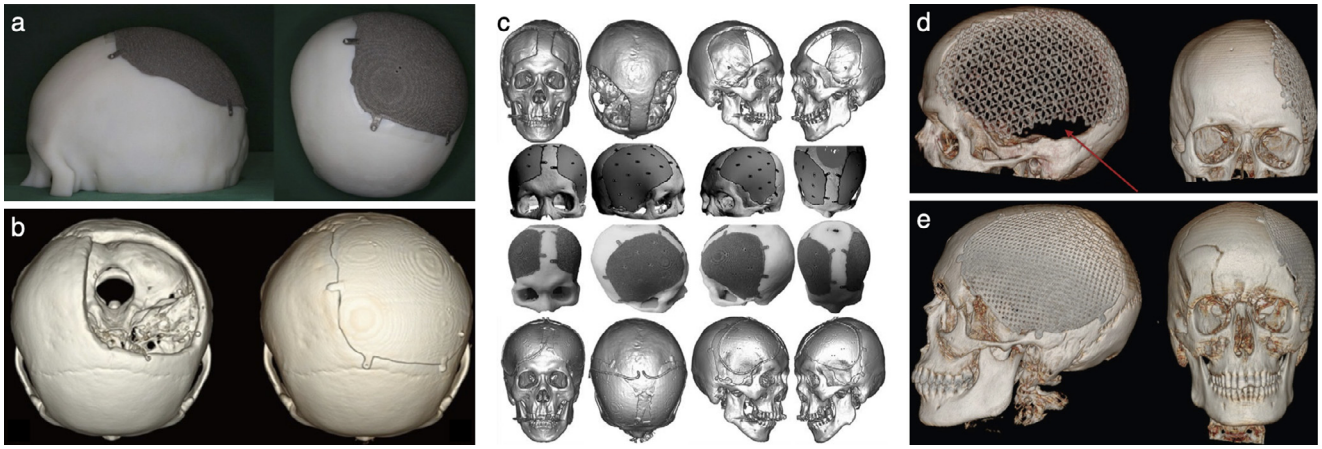

Fig. 4. (a–b) Reconstruction of a large cranial defect. (a) 3D printed prosthesis. (b) Computed tomography, preoperative (left) and postoperative (right). From Cho et al. 2015. Arch Craniofac Surg. Reproduced under the terms of the CC BY-NC 3.0 [54]. (c) Bilateral frontal defect reconstruction. The process involves preoperative imaging (computed tomography), virtual planning, prosthesis manufacture, and postoperative validation. From Park et al. 2016. J Craniofac Surg. Adapted with permission from Wolters Kluwer Health, Inc. [55]. (d–e) Comparison between pre-curved mesh and personalised prosthesis. (d) Pre-curved mesh (CranioCurve, Zimmer Biomet, USA). Incomplete coverage of the cranial defect, persistent defect (red arrow), and unsatisfactory cosmetic result. (e) Personalised prosthesis (MT Ortho, Italy). Complete coverage of the cranial defect and adequate cosmetic result. From Policiccio et al. 2020. Surg Neurol Int. Reproduced under the terms of the CC BY-NC-SA 4.0 [57].

were designed with a honeycomb structure to reduce the weight while retaining acceptable mechanical strength (Fig. 4c) [55]. Similarly, complex reconstructions of frontal-parietal, bifrontal, and pterional skull defects have been performed using EBM constructs without any complications at 1-year follow-up [56]. Compared to the use of a pre-curved titanium mesh graft, custom-made cranial prostheses generally yield better cosmetic results owing to the precise fit in terms of shape and size, in addition to reduced operating time, and greater control over finer anatomical details (Fig. 4d–e) [57]. The same approach shows successful reconstruction of an unusual frontal bone defect in a Parry-Romberg syndrome patient, where the designed prosthesis extended from the superior orbital rim to the vertex [58].

4.2. Mandible and skull base

Mandibular reconstructions typically use autologous bone grafts anchored to the native bone with plates and screws, or in the case of smaller defects, various meshes packed with bone particles or synthetic bone graft substitutes. Although patient-specific implants potentially decrease comorbidities associated with graft harvesting, customisation and load-bearing requirements of mandibular prostheses remain challenging. Among the earliest examples of EBM manufactured mandibular implants in clinical treatment were patient-specific load-bearing plates and titanium meshes with attached fixation plates. Following resections performed by means of custom-made surgical cutting guides, these implants can be *loaded* with an autologous bone graft and bone particulates and/or substitutes [59]. The mandible is also one of the sites most frequently affected by irradiation, which may result in osteoradionecrosis [60]. It has been demonstrated that repair of mandibular fracture secondary to osteoradionecrosis may be successfully achieved with an autologous fibular flap and EBM manufactured patient-specific plates [61]. Larger mandibular reconstructions require additional design features to successfully anchor the custom-made implant and prevent failure under functional loading. One example is of an integrated, diamond-like, porous network in areas of the implant that are in direct contact with native bone. Here, a strut thickness of ~400 μm and pore size in the 600–700 μm range accommodated bone ingrowth and attachment (Fig. 5a–b). At 6-months follow-up, the patient showed an acceptable aesthetic outcome and improved quality of life [62]. In a similar case, individualised mandible implant treatment showed no adverse effects at 14-month follow-up (Fig. 5c–d) [63].

Not surprisingly, custom-made titanium implants show better mandibular contour, symmetry, and function, in addition to fewer postoperative complications following tumour resection compared to conventional titanium plates and fibular autografts [64]. However, custom-made titanium implants for segmental reconstruction of mandibular discontinuity following benign tumour excision are not without challenges. Wound dehiscence (without infection) and development of a persistent extraoral fistula can occur and may require implant removal (Fig. 5e–g) [65]. Patient-specific, EBM manufactured trays filled with iliac crest bone particulates represent a different approach to mandibular reconstruction. Wound dehiscence was reported in some cases, possibly attributable to the large size of the lesion and/or unfavourable geometry of the EBM manufactured tray (Fig. 5h–k) [66]. Extreme facial asymmetry arising from unsuccessful primary reconstruction of a unilateral mandibular defect extending from the mental foramen to the condyle has also been addressed using an EBM fabricated implant. Orthognathic surgery involved aligning the maxilla by a virtually planned Le Fort I osteotomy together with mandibular reconstruction. Prosthesis design integrated a porous design extending 1 cm from the contralateral mandibular bone, and a metal condylar replacement was attached to the remaining solid body. Mechanical testing was performed in order to determine the maximum and fatigue load forces of the implant [67]. Finally, extremely complex reconstructions involving the skull base and the temporomandibular joint have been achieved with patient-specific, multi-component prosthesis involving the skull base, part of the temporal bone (EBM manufactured Ti6Al4V), ramus of the mandible (EBM Ti6Al4V), the glenoid fossa (milled ultra-high-molecular-weight polyethylene), and the mandibular condylar (milled CoCr) (Fig. 5l–p) [68].

4.3. Spine

Customised, self-stabilising vertebral bodies have been used in oncologic resections involving either a single vertebra or multiple vertebrae with a generally acceptable outcome 1-year follow-up [69] (Fig. 6a–b) [70]. Likewise, customised vertebral bodies replacing the C2 vertebrae removed due to primary tumours, showed new bone formation at the last recorded follow-up (Fig. 6c–d). All patients received irradiation therapy postoperatively. While some of the patients were lost to metastatic disease or local recurrence,

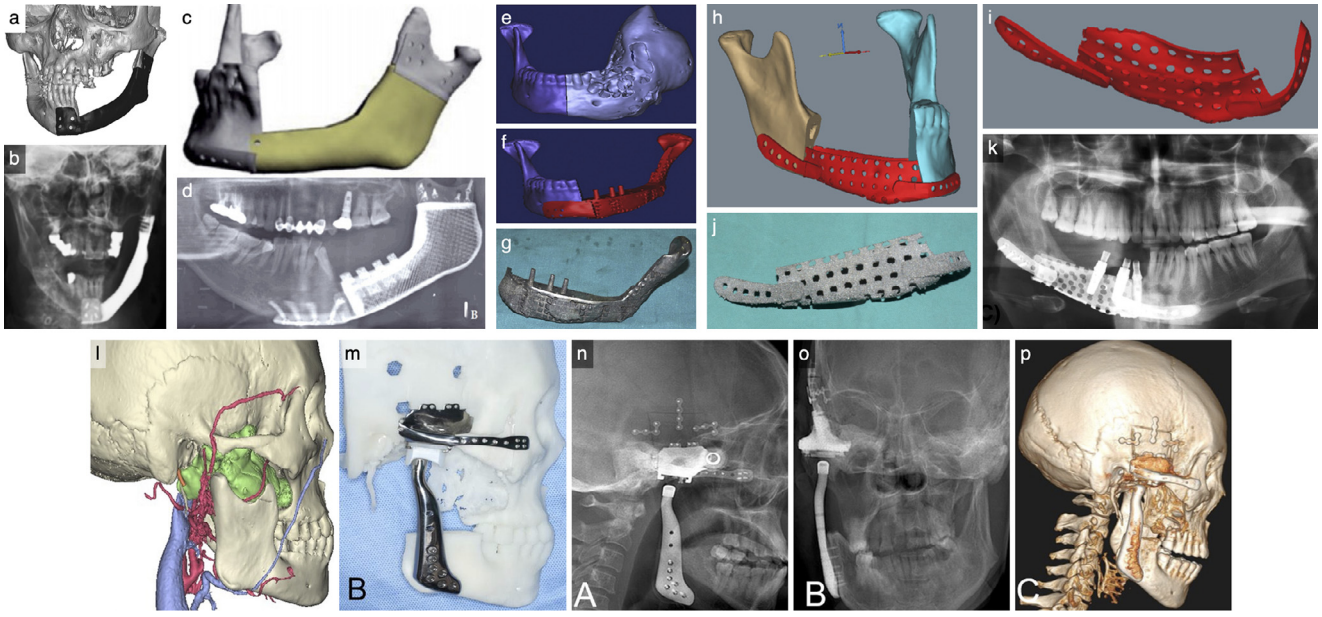

Fig. 5. (a–b) Unilateral mandibular reconstruction. (a) Prosthesis design. (b) Radiograph, postoperative. From Suska et al. 2016. J Oral Maxillofac Surg. Adapted with permission from Elsevier [62]. (c–d) Squamous cell carcinoma. (c) Prosthesis design. (d) Radiograph, 5-months postoperatively. From Lee et al. 2018. Arch Craniofac Surg. Reproduced under the terms of the CC BY-NC 4.0 [63]. (e–g) Benign tumour of the mandible. (e) Computed tomography, preoperative. (f) Simulated matching of residual mandible and prosthesis. (g) 3D printed prosthesis. From Mounir et al. 2020. J Craniomaxillofac Surg. Adapted with permission from Elsevier [65]. (h–k) Follicular ameloblastoma of the anterior mandible. (h) Simulated matching of residual mandible and prosthesis. (i) Prosthesis design. (j) 3D printed prosthesis. (k) Radiograph, 5-months postoperatively. From Farid Shehab et al. 2018. Int J Med Robot. Adapted with permission from John Wiley and Sons [66]. (l–p) Combined skull base and temporomandibular joint prosthesis. (l) Computed tomography of the entire skull, mandible, maxilla, temporomandibular joint, and upper neck. The major blood vessels (red/blue) and the lesion (green) are seen. (m) 3D printed skull base and mandibular ramus components. (n) Radiograph, postoperative (lateral view). (o) Radiograph, postoperative (frontal view). (p) Computed tomography, postoperative. From Zheng et al. 2019. Int J Oral Maxillofac Surg. Adapted with permission from Elsevier [68].

all surviving patients had no signs of implant displacement [71]. For the C1/C2 posterior fusion, a custom fixation implant was used to address facet arthropathy with nerve impingement. 3D printed drill guide assisted in trans-articular screw placement effectively reducing the operative duration. Satisfactory results were reported at 6-months postoperatively [72]. Personalised anterior column cages, composed of an inner lattice structure and an outer shell, connected to a pedicle screw-rod system, were used to replace thoracic and lumbar vertebrae in patients undergoing *en bloc* excision of tumour-affected bone (Fig. 6e–g). In an attempt to address segmental kyphosis, some of the patients received a slightly larger prosthesis than the native bone gap. At the final follow-up, varying degrees of subsidence were noted in all patients, but only one patient required revision surgery for further stabilisation [73]. Cervical spine chordoma affecting the craniocervical junction has been treated with extensive resection and a custom-designed, titanium cage filled with bone matrix, which was additionally stabilised with screws. At 9-month follow-up, radiographic evaluation showed successful fusion [74]. In another case, complex spinal deformity is addressed by a custom, 3D printed, interbody fusion implant that showed no subsidence after one year (Fig. 6h) [74]. A similar approach has been undertaken in an another patient, where lateral lumbar interbody cages were designed to correct vertebral collapse and lumbar lordosis by adding an overall 10° lordosis to the cages (Fig. 6i–m) [75].

4.4. Clavicle, scapula, and sternocostal reconstruction

The whole clavicle, affected by a large osteolytic lesion, may be replaced by a porous prosthesis designed using diagnostic data from contralateral clavicle shape and size (Fig. 7a–b). Certain features (such as small holes) can be introduced into the prosthesis design to enable the attachment of the acromion, sternum, and coracoclavicular ligament [76]. Similarly, successful reconstruction of the entire scapula has been achieved using an EBM manufactured prosthesis following excision due to Ewing's sarcoma (Fig. 7c–d). Small holes incorporated into the prosthesis design allowed suturing of coracoclavicular ligament and surrounding muscles to the implant [76]. An alternative scapular prosthesis design involves circumferential grooves, as to incorporate allogenic bone chips and achieve close attachment of the latissimus dorsi rotational flap following skeletal tumour excision [77]. For partial reconstruction of the scapula, a custom-made prosthesis can also be coupled to an inverse proximal humerus prosthesis [78]. Indicating the uniqueness of such cases, only two customised scapula reconstructions (~ 5%) are reported in a retrospective analysis of custom 3D prostheses used in an 8-year period [79]. Sternocostal reconstructions following large bone resections also benefit from custom-made, 3D printed prostheses. As demonstrated in a patient suffering from primary malignant sternal tumour, a patient-specific sternum prosthesis can also include titanium rods to recreate the ribs allowing for unobstructed respiration with costal stump attachment clamps that assure successful fixation of the prosthetic device (Fig. 7e–h). Here, use of virtual planning and fabrication of a surgical cutting guide enabled precise tumour resection and prosthesis installation [80].

4.5. Shoulder, humerus, radius, and ulna

With the aim to restore upper limb function, a custom-made prosthesis at 60% porosity was designed to replace a loosened total shoulder arthroplasty, originally performed due to chondrosarcoma of the proximal humerus. At 2-year follow-up, function of the joint appeared well-restored and supported daily activities (Fig. 8a–d) [81]. In reverse shoulder arthroplasties, excisions of proximal humerus tumours in patients are addressed with EBM manufactured glenoid prostheses and conventionally made custom humerus prostheses. With a good functional outcome at the final

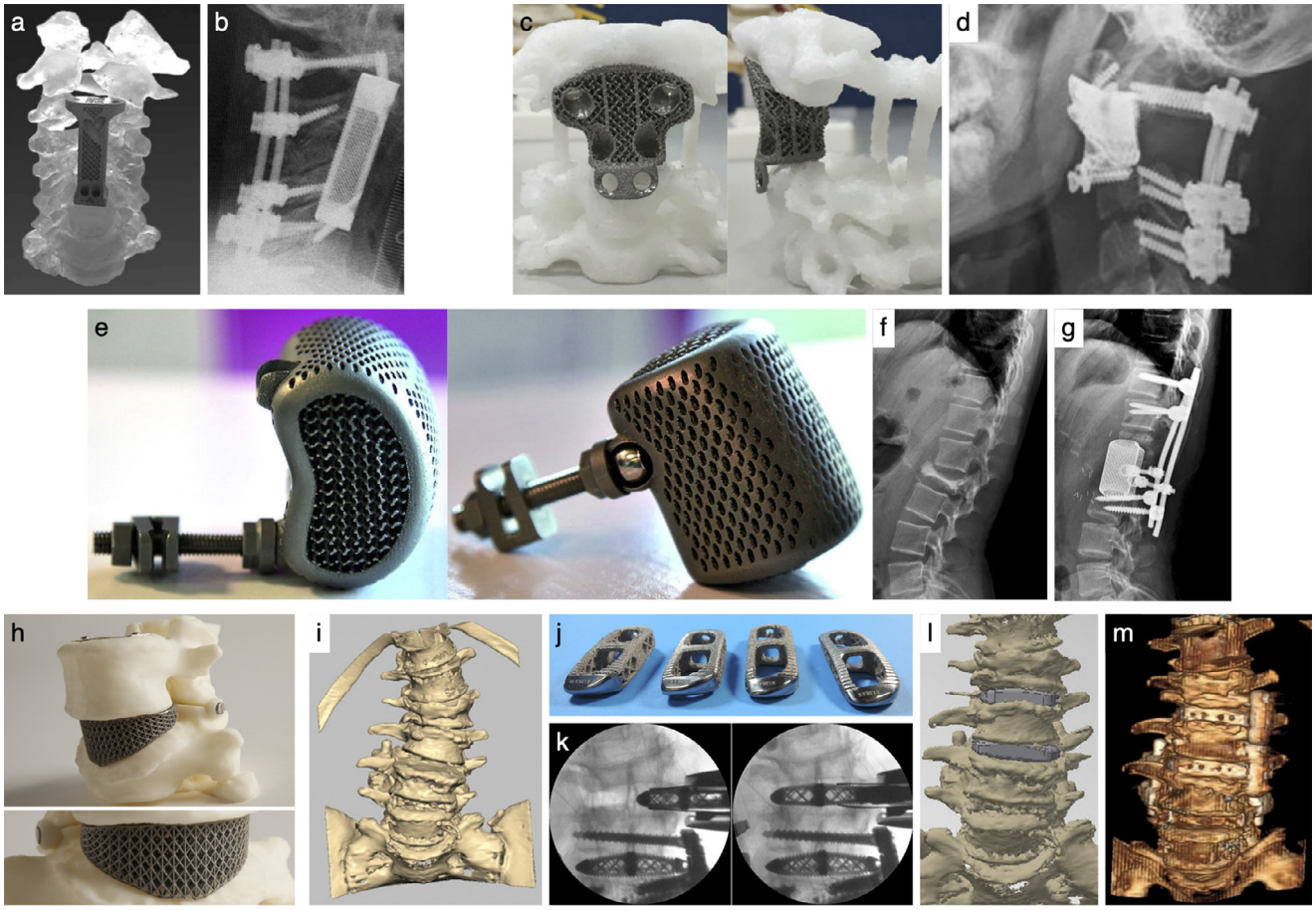

Fig. 6. (a–b) Papillary thyroid carcinoma. (a) 3D printed artificial vertebral body for multilevel reconstruction. (b) Radiograph, postoperative. From Li et al. 2017. Spine (Phila Pa 1976). Adapted with permission from Wolters Kluwer Health, Inc. [70]. (c–d) Giant cell tumour of the cervical spine. (c) 3D printed artificial vertebral body for single vertebra reconstruction. (d) Radiograph, postoperative. From Wei et al. 2020. Ann Transl Med. Reproduced under the terms of the CC BY-NC-ND 4.0 [71]. (e–g) Giant cell tumour of the lumbar spine. (e) 3D printed prosthesis. (f) Radiograph, preoperative. (g) Radiograph, postoperative. From Girolami et al. 2018. Eur Spine J. Adapted with permission from Springer Nature [73]. (h) 3D printed prosthesis for correction of congenital hemivertebra, segmental kyphosis, and loss of lordosis. From Mobbs et al. 2017. J Neurosurg Spine. Images courtesy of Prof. Ralph J. Mobbs, University of New South Wales, Sydney, Australia [74]. (i–m) Lateral recess and foraminal stenosis. (i) Computed tomography of the lumbar spine. (j) 3D printed interbody cages. Processing steps prior to implantation included screw threading, selective polishing, etching, and cleaning. (k) Intraoperative imaging to confirm positioning of the interbody cages. (l) Simulation of vertebral repositioning by interbody cage implantation. (m) Computed tomography, postoperative. From Siu et al. 2018. World Neurosurg. Adapted with permission from Elsevier [75].

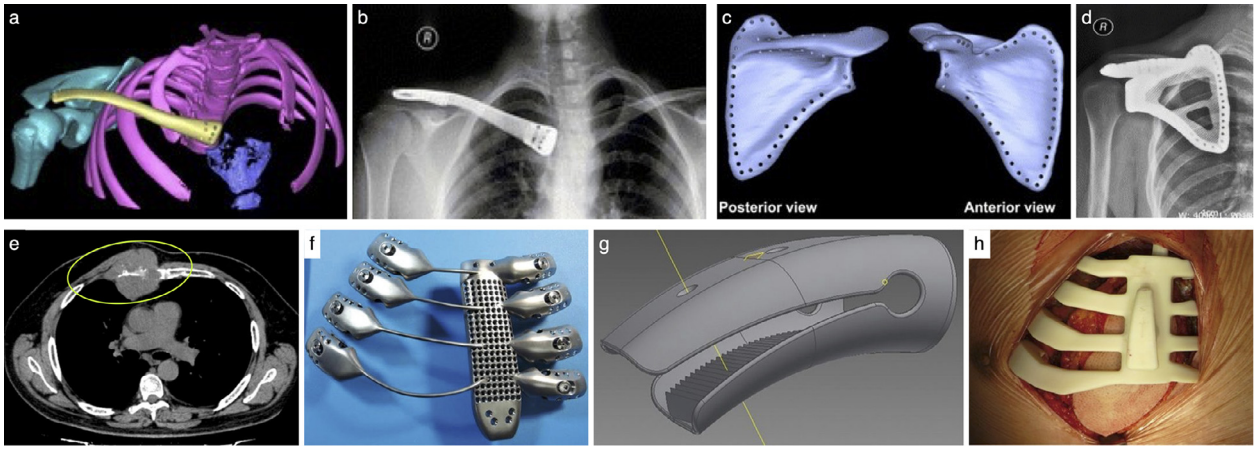

Fig. 7. (a–b) Ewing's sarcoma of the clavicle. (a) Prosthesis design and virtual clavicle reconstruction. (b) Radiograph, 24-months postoperatively. (c–d) Ewing's sarcoma of the scapula. (c) Prosthesis design. (d) Radiograph, 21-months postoperatively. From Fan et al. 2015. World J Surg Oncol. Reproduced under the terms of the CC BY 4.0 [76]. (e–h) Sternal chondrosarcoma and sternocostal reconstruction. (e) Involvement of chest wall structures. Computed tomography. (f) 3D printed implant. (g) Costal stump attachment clamp with a rough inner surface and bolt hole. (h) Surgical template. From Aranda et al. 2015. Eur J Cardiothorac Surg [80].

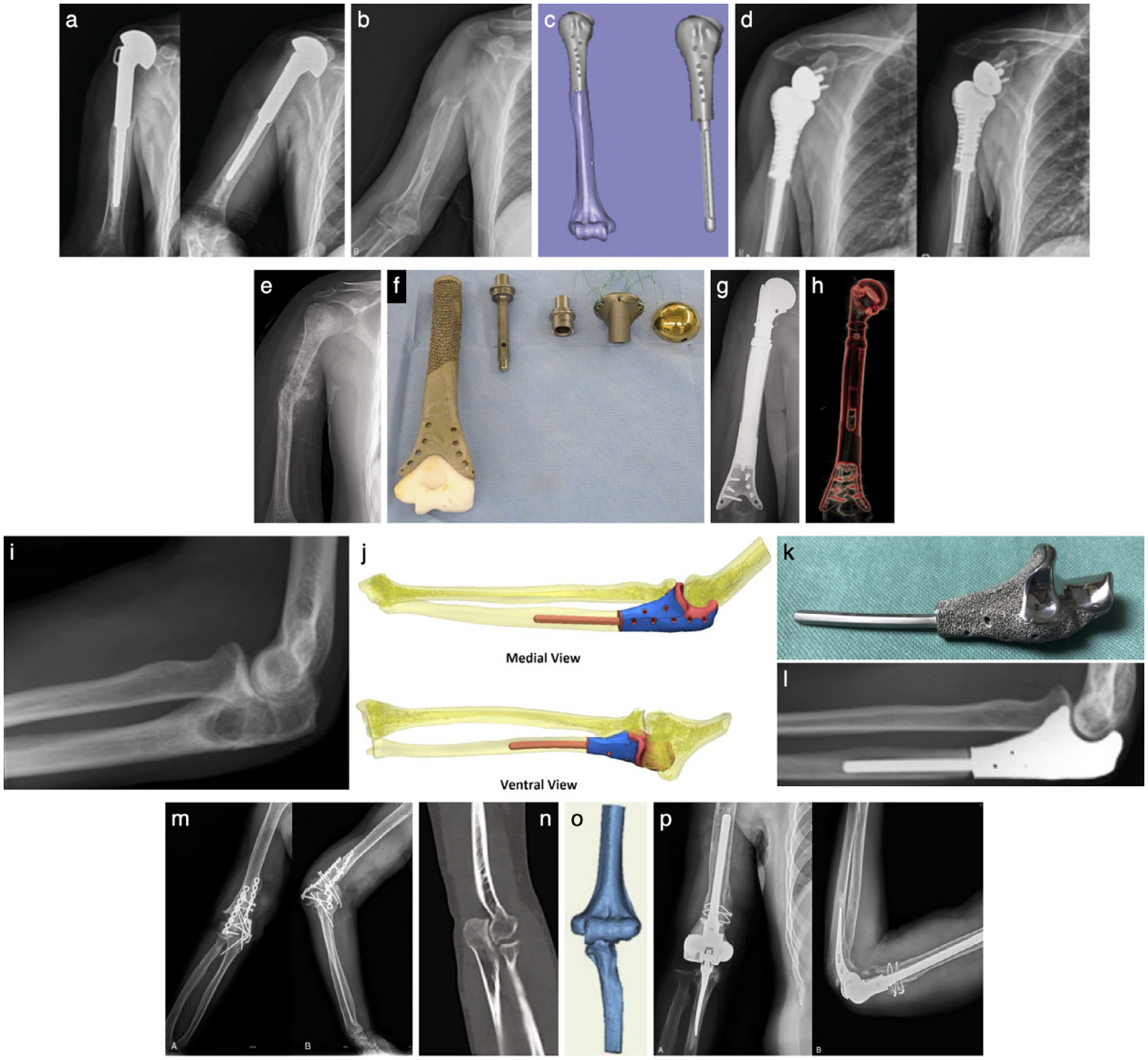

Fig. 8. (a–d) Chondrosarcoma of the proximal humerus. (a) Previous humeral resection and total shoulder arthroplasty. Radiographs. (b) Removed failed previous prosthesis. Radiograph. (c) Prosthesis design. (d) Radiographs, 3-months (left) and 12-months (right) postoperatively. From Zou et al. 2018. Medicine (Baltimore). Reproduced under the terms of the CC BY-NC-ND 4.0 [81]. (e–h) Osteosarcoma of the humerus. (e) Radiograph, preoperative. (f) 3D printed prosthesis. (g) Radiograph, postoperative. (h) Computed tomography showing humeral reconstruction. From Park et al. 2020. Acta Orthop. Reproduced under the terms of the CC BY 4.0 [83]. (i–l) Grade II chondrosarcoma of the proximal ulna. (i) Radiograph, preoperative. (j) Designed prosthesis. (k) 3D printed prosthesis. (l) Radiograph, 30-months postoperatively. From Brandsma et al. 2020. JSES Int. Reproduced under the terms of the CC BY 4.0 [84]. (m–p) Comminuted distal humerus fracture. (m) Fixation failure and non-union after internal fixation. Radiographs. (n) Computed tomography of the intact contralateral limb. (o) Implant design based on mirrored images of the contralateral limb. (p) Radiographs, 36-months postoperatively. From Wu et al. 2020. Medicine (Baltimore). Reproduced under the terms of the CC BY 4.0 [85].

follow-up, no complications associated with shoulder reconstruction were reported [82].

In a one-stage reconstructive surgery during the course of bone tumour treatment, humerus restoration has been performed with custom-made, hollow prostheses that were filled with bone autograft, bone allograft, or an antibiotic cement [77]. In another humeral reconstruction following resection due to osteosarcoma, the elbow joint was preserved with a 3D printed implant designed for use in combination with a conventional modular tumour prosthesis (Fig. 8e–h). The patient retained all functionality below the elbow with minor limitation in shoulder movement [83]. During another effort to avoid complete reconstruction of the elbow joint, a custom-made proximal ulna was manufactured. Accessory holes were incorporated for muscle attachment and the implant was coated with titanium nitride (Fig. 8i–l). Complications included slight sensory loss in the fifth digit. However, the patient was able to function normally at 2.5-year follow-up, with active extension limited to 10° and minor collateral instability, but no problems with flexion or external rotation [84]. Further reconstructions of the radius and ulna have been reported by retrospective studies investigating custom-made 3D printed prosthetic implants [78,79].

Total elbow arthroplasty following a traumatic injury can be carried out with a hinge joint prosthesis encompassing a smaller ulnar stem and a larger humeral stem in line with the extent of the injury (Fig. 8m–p). The range of motion at the elbow joint was between 0° and 135°, together with rotation up to 90° [85].

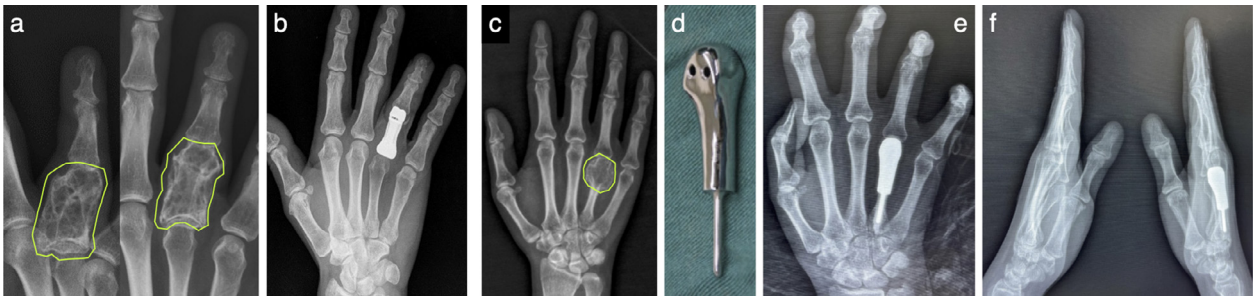

Fig. 9. (a–b) Giant cell tumour at the fourth proximal phalanx. (a) Radiographs, preoperative. (b) Radiograph, 12-months postoperatively. From Beltrami G. 2018. BMJ Case Rep. Reproduced under the terms of the CC BY-NC 4.0 [86]. (c–f) Giant cell tumour of the metacarpal. (c) Radiograph, preoperative. (d) 3D printed prosthesis. (e) Radiograph, 24-months postoperatively (anteroposterior view). (f) Radiograph, 24-months postoperatively (lateral view). From Xu et al. 2021. Ann Transl Med. Reproduced under the terms of the CC BY-NC-ND 4.0 [87].

4.6. Hand (phalanx and metacarpal)

One reported case of phalangeal giant cell tumour reoccurrence necessitated complete excision of the affected phalanx and the articular joint following previous reconstruction with an autologous bone graft. For this purpose, a personalised prosthesis was designed with holes to allow ligament attachment (Fig. 9a–b) [86]. Similarly, personalised EBM manufactured prostheses can be used to address unsatisfactory results achieved by conventional treatments for metacarpal giant cell tumours (Fig. 9c–f). The excised bone was replaced with prostheses having a head-and-handle geometry and a smooth surface [87].

4.7. Pelvis

Anatomically complex pelvis reconstructions following extensive tumour resection also benefit from a personalised medicine approach that EBM has to offer. A promising patient-specific design consists of a solid body with a porous bone-facing surface. Reportedly, early complications in such prostheses include wound dehiscence and failure of adaptation between the prosthesis and the pubic symphysis. Deep infection and systemic sepsis are reported as late complications and may require replacement of the prosthesis with an antibiotic cement spacer [88]. In a similar approach, anatomically conforming hemipelvic prostheses can be designed in a honeycomb-like configuration to reduce the weight of the implant, with a porous bone-facing surface (400–450 µm pore size, 70% porosity) and solid load-bearing regions [89]. In terms of blood loss, length of surgical incision, quality of resection margins, and duration of surgery personalised prostheses offer significant advantages over the conventional nail rod or steel plate systems for pelvic reconstruction [90]. Large, custom-made, hemipelvic prosthesis with a macro-porous bone-facing surface (~400 µm pore size, 60% porosity) adds to the list of successful pelvic reconstructions (Fig. 10a–e) [91]. Similarly, ilium reconstruction using a porous endoprosthesis shows good stability and alignment at 18 months [76]. The combination of 3D printed implants and conventional orthopaedic solutions can also be attempted in pelvic reconstructions. For example, a patient-specific pelvic implant of uniform lattice structure with an acetabular socket at the correct inclination/anteversion and a conventional acetabular cup may be assembled, *ex situ*, prior to insertion [83]. Endoprostheses can be designed so as to allow graft inclusion within a hollow cavity, with the aim to improve vascularisation of the residual bone and likelihood of osseointegration [77].

Sacral osteosarcomas are very rare. The surgical treatment is challenging since adequate surgical margins are difficult to obtain and survival rates remain low [92]. Successful reconstruction of the left hemisacrum following an osteosarcoma excision has been demonstrated with a custom-made prosthesis. The sacrum was cut along the midline, from L2 to the coccyx, and replaced with a porous Ti6Al4V prosthesis. Bone ingrowth and fusion with the residual right sacrum were noticeable by one year postoperatively [93]. Depending on the extent of tumour growth, custom-made hemipelvic endoprostheses with acetabular components can be used in reconstructions involving the ilium, acetabulum, pubis, and ischium. Prostheses having both solid areas and porous structures, at 600 µm pore size and 70% porosity, have been found to be useful. Where complete acetabulum excision was needed, attachment to the pubis was achieved with either a pubic stem or a 'cap-like' connection. Here, no severe complications were reported at ~2-year follow-up [94].

Partial and complete pubis restoration following a chondrosarcoma excision can be achieved using prostheses with and without a pubic symphysis traversing stem. Specifically for prostheses without a stem, porous structures (600 µm pore size, 70% porosity) were introduced at the pubis-ilium and pubis-ischium interfaces. No implant failure or recurrent disease was reported at 24-month follow-up (Fig. 10f–k) [95,96]. In two cases of periacetabular Ewing's sarcoma (in a 6- and an 8-year-old), excision was carried out via a trans-acetabular osteotomy based on the 'triradiate cartilage strategy'. Here, the prostheses were designed not to mimic the original anatomy, but to optimise function (Fig. 10l–p). Loading forces on the prostheses were examined by simulating the conditions of various activities including walking, single leg standing, standing up, sitting down, ascending, and descending stairs in a finite element model. The topology was thus optimised by reducing the bulk of the prosthesis and removing unnecessary material from minimally load-bearing regions [97]. In pelvic reconstructions after bone tumour, the proximal resection levels of the ilium may be used as a guide to design the prosthesis. For instance, in resections that involve the entire iliac bone or part of the sacrum, spinopelvic fixation of the 3D printed prosthesis has been recommended [78]. The overall success rate of pelvic reconstructions varies and is difficult to compare as it involves a wide range of confounding factors. In a large study where the majority of cases involved pelvic reconstruction, wound dehiscence was the most frequent complication with good functional results in 85% of the cases [79].

4.8. Hip, femur, and tibia

Massive acetabular bone loss due to periprosthetic joint infection has been addressed with a two-stage hip revision using custom-made acetabular implants with an overall implant survival of 95%. Acetabular components were designed with a thick porous structure on the exterior and a wide porous structure on the interior of the implant. In some cases, flanges were added for better fixation [98]. Preoperative planning of centre of rotation and inclination, in custom-made acetabular components with bone facing trabecular regions, can be highly valuable in minimising peripros-

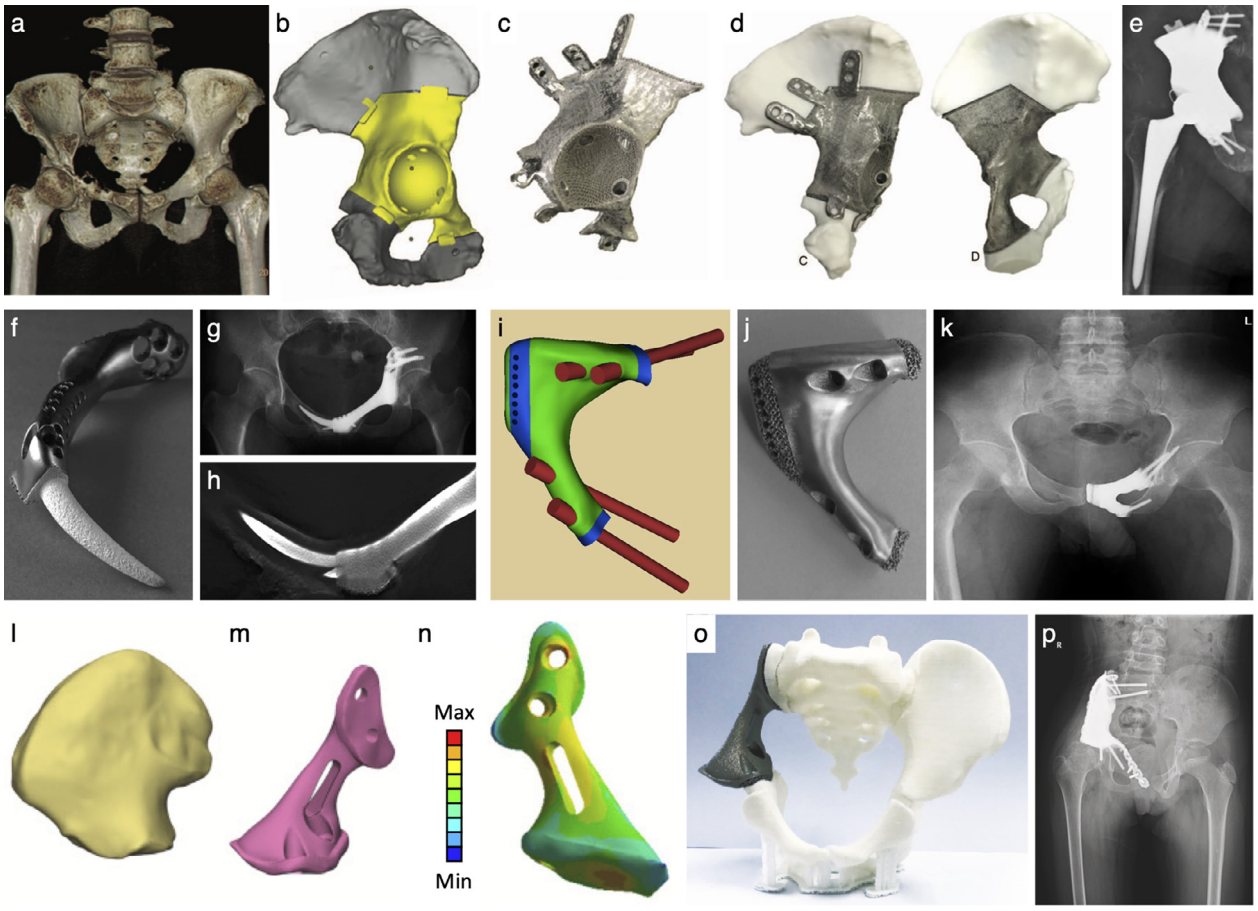

Fig. 10. (a–e) Metastatic acetabulum carcinoma. (a) Computed tomography, preoperative. (b) Simulated matching of residual hemipelvis and pelvic prosthesis. (c) 3D printed prosthesis (d) Preoperative fitting and 3D printed prosthesis. (e) Radiograph, 3-months postoperatively. From Han et al. 2019. Medicine (Baltimore). Reproduced under the terms of the CC BY-NC-ND 4.0 [91]. (f–h) Prosthesis with a medullary stem for insertion into the pubis. (f) 3D printed prosthesis. (g) Radiograph, 6-months postoperatively. (h) Fretting wear around medullary stem (tomosynthesis). From Zhang et al. 2021. BMC Musculoskelet Disord. Reproduced under the terms of the CC BY 4.0 [96]. (i–k) Prosthesis comprising solid and porous structures and four fixation screws. (i) Prosthesis design. (j) 3D printed prosthesis. (k) Radiograph, 2-months postoperatively. From Zhang et al. 2020. J Orthop Surg Res. Reproduced under the terms of the CC BY 4.0 [95]. (l–p) Periacetabular Ewing's sarcoma. (l) Anatomically accurate prosthesis design. (m) Reduced volume prosthesis design achieved via topology optimisation. (n) Finite element simulation of loading. (o) Preoperative fitting of 3D printed prosthesis. (p) Radiograph, 48-months postoperatively. From Zhu et al. 2021. J Orthop Translat. Reproduced under the terms of the CC BY-NC-ND 4.0 [97].

thetic failure. For example, only one failure is reported during 12–40 month follow-up of large acetabular bone defect reconstructions [99]. Single case of acetabular bone defect in developmental dysplasia of the hip was resolved with customised acetabular prosthesis that simultaneously addressed the underlying bone defect and restored the hip rotation centre. No radiolucency or acetabular cup migration was noted at 12-month follow-up [100].

Custom 3D printed prostheses are also successfully used in the correction of irregularly shaped femoral defects caused by trauma or infection via a two-step approach. First, the defects are removed and a temporary fixation is put in place. Second, a custom-made hollow-body prosthesis mimicking the size and shape of the original bone, with a dodecahedron pore design (~625 µm pore size, 70% porosity), is affixed to the remaining bone using intramedullary nail fixation [101]. Other potential implant designs for femoral reconstructions include solid body with a lattice structure coating (Fig. 11a–d), or a two-part mesh body that wraps around the native bone and is held into position with intramedullary nail fixation and bone cement (Fig. 11e–h) [83].

Reconstructions of proximal tibiae following tumour resection are also frequently undertaken. Prostheses designs have taken into consideration the morphological appearance of corresponding healthy tibia, attachment of collateral ligaments, and incorporation of standard knee prostheses so that a medullary stem can be inserted through the 3D printed block (Fig. 11i) [102]. Where knee joints are preserved, the resected bone is replaced by patient-specific proximal tibial prostheses. Implants have been manufactured so that the bone-facing surface and areas of patellar tendon attachment are porous (450–550 µm pore size and 60% porosity) [103]. In one case of preserved knee joint after subchondral giant cell tumour removal, a two-part porous implant was designed to support subchondral graft in the tibial epiphysis and maintain proper articulation of the knee. A *bearing-plate* and a *strut* were connected together through a specialised slideway, and the strut was fixed by screws to the tibial cortex (Fig. 11j–k) [104]. In cases of malignant primary bone tumour invading intercalary tibia, prostheses with highly cancellous surface to promote tissue ingrowth were custom-designed (Fig. 11l–o) [105]. A personalised, two-part *mega-endoprosthesis* was designed to accommodate preservation of the knee joint following chronic allograft rejection (Fig. 11p–s). An EBM manufactured head with trabecular structure (65% porosity) was attached to the cortex of the tibial plate, and a stem produced by traditional casting to ensure mechanical stability by press fitting into the distal tibia [106].

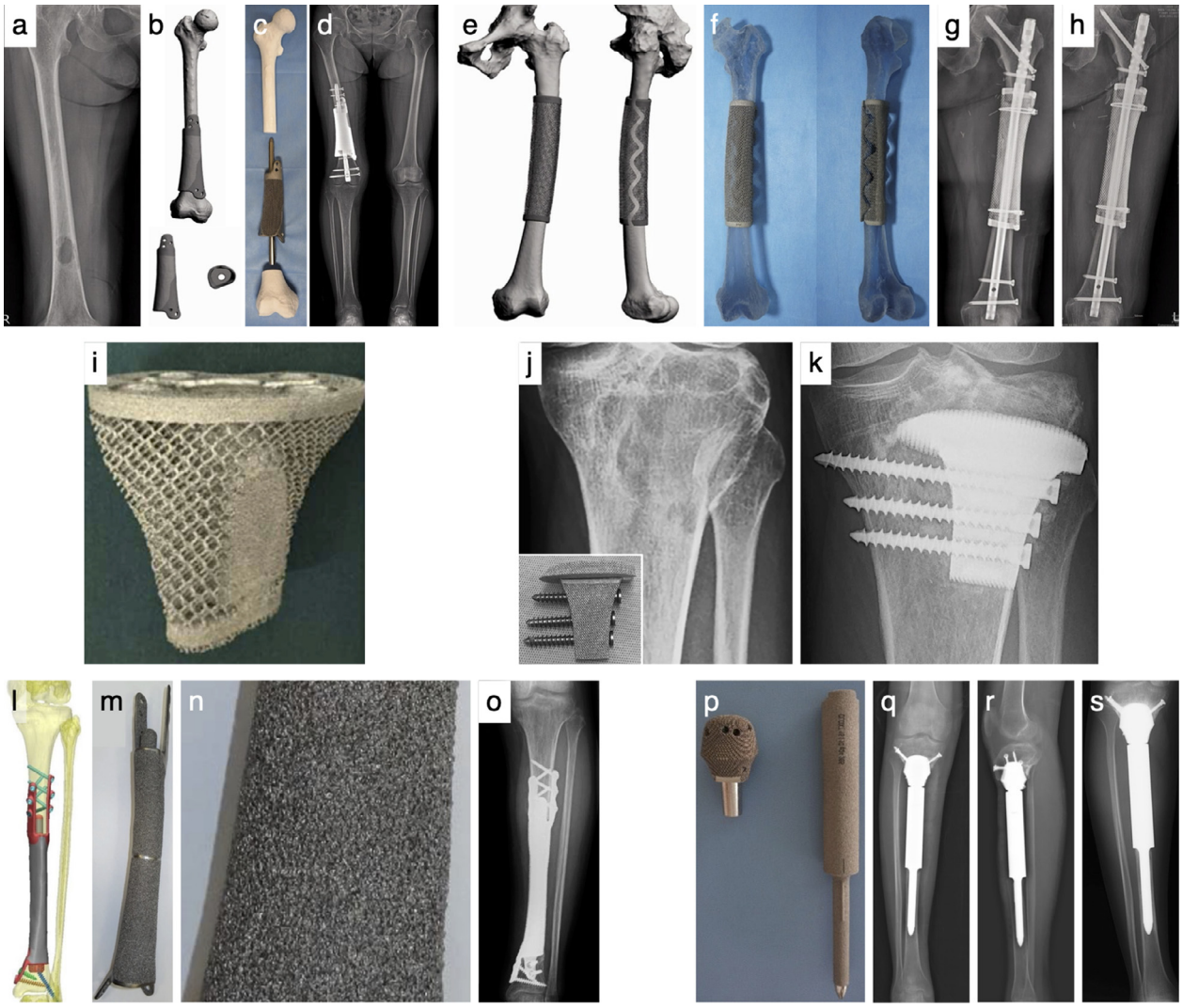

Fig. 11. (a–d) Undifferentiated pleomorphic sarcoma of the femur. (a) Radiograph, preoperative. (b) Prosthesis design. (c) 3D printed prosthesis. (d) Radiograph, postoperative. (e–h) Femoral metastasis of renal cell carcinoma. (e) Prosthesis design. (f) 3D printed prosthesis. (g) Radiograph, postoperative. (h) Radiograph, 3 months postoperatively. From Park et al. 2020. Acta Orthop. Reproduced under the terms of the CC BY 4.0 [83]. (i) 3D printed prosthesis for proximal tibia reconstruction. From Luo et al. 2017. Med Sci Monit. Reproduced under the terms of the CC BY-NC-ND 4.0 [102]. (j–k) Giant cell tumour of the proximal tibia. (j) Radiograph, preoperative. Inset in j: Prosthesis consists of a bearing plate and strut with three screw holes. (k) Radiograph, 29-months postoperatively. From Lu et al. 2019. BMC Surg. Reproduced under the terms of the CC BY 4.0 [104]. (l–o) Intercalary distal tibia implant. (l) Prosthesis design. (m) Solid implant with a highly porous surface and extracortical plates having interlocking screws. (n) Magnified view of the porous surface. (o) Radiograph, postoperative. From Guder et al. 2021. J Pers Med. Reproduced under the terms of the CC BY 4.0 [105]. (p–s) Multi-component prosthesis for tibial reconstruction. (p) 3D printed proximal part and cast stem. (q) Radiograph, postoperative (anteroposterior view). (r) Radiograph, postoperative (lateral view). (s) Radiograph, 26-months postoperatively. From Lu et al. 2018. World J Surg Oncol. Reproduced under the terms of the CC BY 4.0 [106].

4.9. Foot (phalanx, talus, and calcaneus)

Proximal phalangeal prosthesis was used in a phalanx reconstruction of the fifth toe following removal of the osteolytic lesion attributable to giant cell tumour. Despite initially satisfactory clinical outcomes (including normal weight bearing of the fifth metatarsal head), a dorsiflexion contracture of the toe developed after 8 months and progressed to a full-fixed, overriding toe deformity by 18–24 months (Fig. 12a–e) [107]. Total talar replacement following avascular necrosis allows preservation of tibiotalar articulation. Using EBM manufactured CoCr talar implants, with or without a titanium nitride coating, complete talar replacement was performed with significant improvement in patient-reported outcomes [108]. Similar results are reported in a retrospective study involving patients undergoing the same procedure [109]. In a single-case study using 3D printed talar implant, improved gait is reported at a one year postoperative follow-up [110]. EBM manufactured, nickel-plated, CoCr implants used in complete talar replacement are also capable of maintaining anatomical alignment of the ankle [111]. Total talar replacement, necessitated by osteosarcoma excision, has also been performed with a 3D printed talar prosthesis made from medical-grade titanium. The prosthesis design incorporated features such as tunnels to attach the deltoid ligament, anterior talofibular, and talonavicular ligament (Fig. 12f–i) [112]. In two patients that previously underwent ankle replacement, custom-made total talar prostheses were used following aseptic talar collapse. In one patient, the talar prosthesis was designed to custom-match the corresponding polyethylene surface of the ankle prosthesis, while the second patient underwent total ankle revision with a custom-made talar component (Fig. 11j) [113].

The calcaneus is the largest bone in the foot with a significant role in weight bearing and stability. In the case of a chondrosarcoma resection requiring total calcaneus replacement, a personalised prosthesis was fabricated with anchor points to which the Achilles tendon, plantar fascia, and the spring ligament could be attached [114]. In a similar case of calcaneal desmoplastic fibroma,

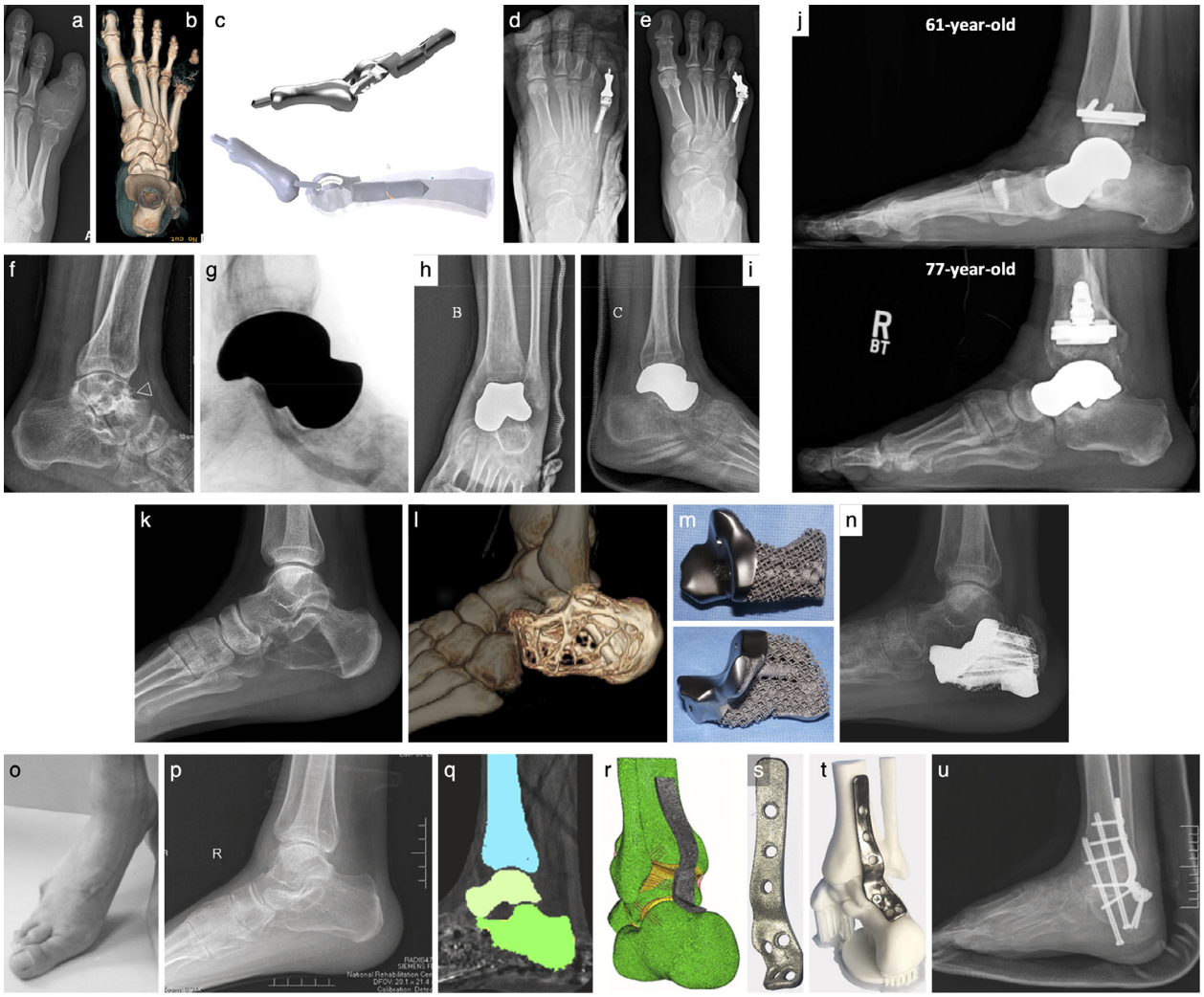

Fig. 12. (a–e) Giant cell tumour of the fifth toe. (a) Radiograph, preoperative. (b) Computed tomography. (c) Prosthesis design. (d) Radiograph, postoperative (anteroposterior view). (e) Radiograph, 24-months postoperatively (anteroposterior view). Overriding toe due to contracture of scar tissue. From Chandhanayingyong et al. 2020. Int J Surg Case Rep. Reproduced under the terms of the CC BY 4.0 [107]. (f–i) Collapse of the left talus. (f) Radiograph, preoperative (lateral view). (g) Intraoperative imaging to confirm positioning of the implant. (h) Radiograph, postoperative (anteroposterior view). (i) Radiograph, postoperative (lateral view) From Huang et al. 2021. J Foot Ankle Surg. Adapted with permission from Elsevier [112]. (j) Total talus arthroplasty in a 61-year old and a 77-year old. Radiographs, 36-months postoperatively. From Strand et al. 2022. Foot Ankle Surg (N Y). Reproduced under the terms of the CC BY-NC-ND 4.0 [113]. (k–n) Desmoplastic fibroma of the calcaneus. (k) Radiograph, preoperative (lateral view). (l) Computed tomography. (m) 3D printed implant. (n) Radiograph, 16-months postoperatively (lateral view). From Park et al. 2018. JBJS Case Connect. Adapted with permission from Wolters Kluwer Health, Inc. [115]. (o–u) Bilateral drop foot. (o) Photograph of right foot, preoperative. (p) Radiograph, preoperative (lateral view). (q) Computed tomography (cross-section view). (r) Finite element simulation of the gait cycle with the designed fixation plate. (s) 3D printed fixation plate. (t) Preoperative fitting of the 3D printed fixation plate. (u) Radiograph, 3-months postoperatively (lateral view). From Yao et al. 2021. Comput Biol Med. Reproduced under the terms of the CC BY-NC-ND 4.0 [116].

a patient-specific prosthesis was designed to preserve the Achilles tendon insertion site. The articular surface, heel pad, and implant body were solid, while a 2 mm mesh was used on the remaining surface of the implant (Fig. 12k–n). The meshed surface was used for attachment of necessary ligaments and soft tissues. Mechanical testing of the prosthesis measured maximal compression load of 2700 kg, which is well above the requirements of everyday dynamic forces [115]. In a tibiotalocalcaneal arthrodesis procedure, personalised plates were designed according to the patient's ankle morphology, and optimised with finite element modelling to withstand physiological loading (Fig. 12o–u) [116].

5. Histological evidence of osseointegration

The bone-implant interface is a '*wide zone within which many complex physical and chemical interactions take place between the surface of the implanted device and the surrounding physiological system*' [117,118]. Absence of relative motion between the implant surface and surrounding tissues under functional loading is a key consideration in achieving osseointegration [119,120]. Having a surface roughness at least an order of magnitude greater than traditional surface modification methods (including acid etching and anodic oxidation), experimental studies routinely show promising results for EBM manufactured Ti6Al4V [34,121] and CoCr [38,39,122] constructs, both with or without integrated macro-porous architecture. Since osseointegrated implants are generally not removed for *ex situ* analysis, only a handful of clinical studies have been able to perform histological evaluation to definitively verify osseointegration, albeit without detailed characterisation of peri-implant bone quality.

Compared to conventionally manufactured acetabular cups, lamellar bone ingrowth is observed more frequently in EBM manufactured acetabular cups suggesting that the bone remodelling process is undisturbed [43]. Histological assessment of EBM manu-

factured hemipelvic endoprosthesis retrieved due to reoccurrence of osteosarcoma also reveals significant bone ingrowth into the porous layer, although some regions largely contained fibrous or loose connective tissue [48].

The use of EBM manufactured plates together with an autologous fibular flap has been found to be a valuable strategy for the repair of mandibular fracture. During functional rehabilitation (i.e., to allow for dental reconstruction), *en bloc* retrieval of an EBM manufactured plate together with associated bone enabled histological assessment of both the fibular flap and the native bone. Here, normal turnover of peri-implant bone and close adaptation (i.e., bone-implant contact) of new bone to the EBM manufactured plate was indicative of successful osseointegration [61].

6. The need for bespoke implants – challenges for the future

Besides the traditional applications of bone-anchored metal/alloy implants in dental and orthopaedic applications, the major need for patient-specific and customised implants is in rehabilitation after oncological resection. Many of such patients receive radiotherapy. It is well-known that implants placed in irradiated bone tend to be more susceptible to failure than those in non-irradiated bone [123,124]. Animal experiments corroborate clinical findings, showing lower bone-implant contact, greater peri-implant bone resorption together with fibrotic changes, and reduced implant stability in irradiated bone [125,126]. Irradiation-induced deleterious effects on osseointegration are found to be dose dependent and are primarily attributed to clinically relevant therapeutic doses (> 50 Gy), which correspond to single doses of ~20 Gy and higher in small animals [127–129]. Furthermore, morphological observations of compromised osseointegration after exposure to radiation have been noted at both the early [125] and late [126] periods of healing. But interestingly, delaying implant insertion following irradiation may help to offset the detrimental effects of therapeutic radiation on osseointegration and bone material properties [130]. A large proportion of patients receiving personalised, EBM manufactured prostheses have suffered bone insufficiency owing to oncological resection (Table 1). However, clinical studies have largely failed to report the duration between the most recent dose of irradiation and prosthetic reconstruction. It is also unclear if patients have continued to receive adjuvant radiotherapy after implant insertion. Therefore, long-term success (or failure) of such patient-specific implants and the specific effects of irradiation on bone material properties, bone ingrowth into macro-porous geometries, and bone remodelling currently remain challenging to discuss with a great degree of certainty.

Trabecular bone is neither random, nor a perfect '*lattice*'. In fact, the microstructure of trabecular bone is often characterised as a collection of plate-like and rod-like trabeculae [131]. In this regard, EBM provides an opportunity to more accurately replicate trabecular architecture. Changes in trabecular architecture due to age and presence of disease (e.g., osteoporosis) may be accommodated in the design of EBM-manufactured constructs. Age-dependent changes include increased intracortical porosity with associated with cortical thinning as a result of transformation of the inner cortex into a trabecularised network of cortical bone remnants [132]. However, a practical limitation to achieving a realistic trabecular strut geometry is the size of the powder particles used (~100 μm). Slender, yet mechanically-competent struts can be challenging to achieve with large powder particles.

Additive manufacturing using EBM allows a wide range of open-cellular implant designs to be fabricated in order to eliminate stress shielding and associated bone resorption, and the ability to utilise cementless surgical insertion as well as the enhanced, associated osseointegration and bone formation [5,14]. The ability to fabricate graded porosity can functionalise the implant in a manner similar to natural bone [5]. In certain situations, it is desirable to add a thin coating, such as titanium nitride, on an EBM manufactured component or prosthesis in order to improve wear resistance and/or prevent an allergic response. Preclinical, *in vitro* studies have shown these to be biocompatible, without posing adverse effects on cell proliferation or differentiation [133]. Key examples include the endoprostheses in the vicinity of the elbow joint, and complete replacement of the phalanx and scaphoid [52,53,84,86]. In contrast, nickel-plated CoCr implants may be cause for some concern [111]. Further attesting to the adaptability of EBM, the prosthesis design for a given application can be easily evolved once problems (e.g., fretting wear) are detected [95]. Other interesting uses of EBM include fabrication of custom-made surgical cutting guides for resection [59], which are thought to provide safer surgical margins [79].

Titanium (and titanium alloys) have lower density (~4.4 g/cm^3) compared to CoCr (~8.4 g/cm^3) [14], and therefore the Young's modulus is closer to that of cortical bone. Furthermore, Co is potentially toxic and hence there may be concerns around the use of Co-containing alloys in biomedical applications [134]. Alternatives to metal implants such as polyether ether ketone (PEEK) offer certain physical characteristics (e.g., Young's modulus) that are closer to bone. Nevertheless, the major advantage of macro-porous cp-Ti, Ti6Al4V, and CoCr implants is that osseointegration can be achieved without the addition of bioactive constituents such as hydroxy(l)apatite that are typically added to PEEK [135,136].

Complex shaped implants pose a major challenge in terms of mechanical testing and quality assurance. While standard shaped specimens can be used in mechanical testing machines, for example to investigate the influence of lattice design [137], complex shaped implant specimens cannot be tested in the same manner. Here, finite element modelling can be extremely valuable for testing the mechanical behaviour of implant, as designed, under simulated physiological loading [97,116]. Another possibility is to combine non-destructive imaging such as X-ray computed tomography and numerical simulation for quality control [138] and failure prediction [139].

The cosmetic aspects of skeletal reconstructions (i.e., accuracy of implant fitting) also warrant standardisation. The cosmetic outcome depends on, in addition to other factors, the severity of initial skeletal deformity (loss of function) and the type of prosthesis. Where the defect occurs unilaterally, design of the patient-specific implant can be based on the contralateral body part, as in cases of scapular, clavicular [76], mandibular [62], or tibial [102] reconstructions. Assessment of morphological symmetry of radius and ulna showed small regional differences between contralateral sides (around 0.5 mm) with no statistical difference in length, volume, bowing, or twisting between the two sides [140]. This suggests that contralateral body parts can be used as a point of reference in both implant design and in cosmetic outcome assessment. Digital photography coupled with standardised, quantitative assessment over the entire range of motion, with or without machine learning approaches, can pave the way towards benchmarking cosmetic outcomes. Certain cases, for example reduced volume prostheses designed primarily based on finite element simulation of loading [97], cannot be expected to yield a favourable cosmetic outcome. Here, patient-reported health surveys, such as SF-36 (Short Form Health Survey) containing both physical and mental component summaries, together with assessment of standardised photographs by objective clinical observers can be used. In reconstruction of large cranial defects improved cosmetic result was directly associated with the precise fit of the custom-made prosthesis with cosmetic results assessed by patients using a visual scale for cosmesis [57].

Clinical diagnostic methods such as magnetic resonance imaging and computed tomography are suboptimal for obtaining infor-

Table 1
Summary of the published literature.

Reason	Type	Material	Implant	No. of patients	Follow-up (in months)	Refs.
Onc ($n = 2$), Non-onc ($n = 2$)	*patient-specific*	Ti6Al4V ELI	Plates and meshes for mandibular reconstruction	4	NR	[59]
Onc ($n = 1$), Non-onc ($n = 2$)	*patient-specific*	titanium#	Skull prosthesis	3	4.67	[54]
Onc	*patient-specific*	Ti6Al4V	Clavicular, scapular, and hemipelvic prostheses	3	21	[76]
Onc	*patient-specific*	titanium alloy	Sternocostal prosthesis	1	1	[80]
Onc	*patient-specific*	titanium#	Calcaneus prosthesis	1	5	[114]
Onc	*patient-specific*	Ti6Al4V	Self-stabilising artificial vertebral body	1	12	[69]
Onc	*patient-specific*	Ti6Al4V	Plate for mandibular reconstruction	1	33	[61]
Onc	*patient-specific*	Ti6Al4V	Mandibular prosthesis	1	9	[62]
Non-onc	*patient-specific*	Ti6AL4V ELI	Skull prosthesis	21	11.43	[55]
Non-onc	*patient-specific*	titanium alloy#	Spinal posterior fixation implant	1	2	[72]
Onc	*patient-specific*	Ti6Al4V ELI	Mandibular prosthesis	1	NR	[67]
Onc	*patient-specific*	Ti6Al4V	Self-stabilising artificial vertebral body	1	12	[70]
Onc	*patient-specific*	Ti6Al4V	Hemisacral prosthesis	1	12	[93]
Onc ($n = 1$), Non-onc ($n = 1$)	*patient-specific*	titanium#	Self-stabilising artificial vertebral cage, Interbody fusion cage	2	12	[74]
Non-onc	*patient-specific*	titanium#	Skull prosthesis	10	12	[56]
Onc	*patient-specific*	Ti6Al4V	Tibial prostheses	4	7	[102]
Onc	*off-the-shelf*	titanium alloy#	Hemipelvic prostheses	35	20.5	[47]
Onc	*patient-specific*	Ti6Al4V	Spinal anterior column prostheses	13	up to 18	[73]
Non-onc	*patient-specific*	Ti6Al4V	Interbody fusion cage	1	6	[75]
Onc	*patient-specific*	Ti6Al4V ELI	Mandibular prosthesis	1	14	[63]
Onc	*patient-specific*	titanium#	Mandibular tray prostheses	8	12	[66]
Onc	*patient-specific*	Ti6Al4V	Reverse shoulder prosthesis	1	24	[81]
Onc	*patient-specific*	titanium alloy#	Tibial prosthesis	1	26	[106]
Onc	*patient-specific*	titanium alloy#	Femoral and tibial prostheses	12	22.5	[103]
Onc	*patient-specific*	titanium alloy#	Phalangeal prosthesis, hand	1	24	[86]
Non-onc	*patient-specific*	titanium#	Skull prosthesis	1	6	[58]
Onc	*patient-specific*	Ti6Al4V ELI	Calcaneus prosthesis	1	16	[115]
Non-onc	*off-the-shelf*	Ti6Al4V	Fixation pins for femoral head	30	24	[49]
Onc ($n = 10$), Non-onc ($n = 3$)	*patient-specific*	titanium#	Hemipelvic, scapular, ulnar, radial, calcaneus, tibial, femoral prostheses	13	6–26	[78]
Onc	*patient-specific*	Ti6Al4V, UMHWPE, CoCrMo	Temporomandibular joint combined prosthesis	5	13.8	[68]
Non-onc	*off-the-shelf*	Ti6Al4V	Acetabular cups	9864	range of 96	[44]
Onc	*patient-specific*	titanium alloy#	Hemipelvic prosthesis	1	12	[91]
Onc	*patient-specific*	titanium alloy#	Reverse shoulder prosthesis	7	23.6	[82]
Onc	*patient-specific*	titanium alloy#	Hemipelvic prostheses	13	25.3	[94]
Non-onc	*patient-specific*	CoCr	Talar prosthesis	14	5	[111]
Onc	*patient-specific*	NR	Tibial prosthesis	1	29	[104]

(*continued on next page*)

Table 1 (*continued*)

Reason	Type	Material	Implant	No. of patients	Follow-up (in months)	Refs.
Onc	*off-the-shelf*	titanium[#]	Modular hemipelvic prostheses	80	32.5[†]	[48]
Onc	*patient-specific*	Ti6Al4V	Hemipelvic prostheses	6	18–42	[89]
Onc (n = 34), Non-onc (n = 7)	*patient-specific*	titanium[#]	Hemipelvic, scapular, ulnar, radial, calcaneus, tibial, femoral prostheses	41	20	[79]
Non-onc	*patient-specific*	titanium[#]	Acetabular prostheses	19	42.3	[98]
Non-onc	*patient-specific*	titanium[#]	Acetabular prostheses	20	25.5[†]	[99]
Non-onc	*patient-specific*	titanium[#]	Femoral prostheses	5	16.4	[101]
Non-onc	*patient-specific*	CoCr	Talar prostheses	27	22.2	[108]
Onc	*patient-specific*	Ti6Al4V	Mandibular prostheses	4	12	[64]
Onc	*patient-specific*	Ti6Al4V	Mandibular prostheses	7	48	[65]
Onc (n = 9), Non-onc (n = 1)	*patient-specific*	Ti6AL4V ELI	Hemipelvic, femoral, and humeral prostheses	10	16.3	[83]
Non-onc	*patient-specific*	Ti6AL4V ELI	Skull prosthesis	10	27	[57]
Onc	*patient-specific*	titanium alloy[#]	Phalangeal prosthesis, foot	1	24	[107]
Non-onc	*off-the-shelf*	Ti6Al4V	Acetabular cups	6	*retrieved*	[42]
Onc	*patient-specific*	Ti6Al4V	Self-stabilising artificial vertebral body	9	28.6	[71]
Non-onc	*off-the-shelf*	Ti6Al4V	Acetabular cups	92	48.2	[45]
Non-onc	*patient-specific*	Ti6Al4V	Elbow prosthesis	1	36	[85]
Non-onc	*patient-specific*	Ti6Al4V	Acetabular prosthesis	1	12	[100]
Onc	*patient-specific*	NR	Hemipubic prostheses	5	13.6	[95]
Non-onc	*patient-specific*	titanium alloy[#]	Scaphoid prosthesis	1	12	[53]
Non-onc	*patient-specific*	CoCr	Talar prostheses	15	12.8	[109]
Non-onc	*off-the-shelf*	Ti6Al4V	Acetabular cups	7	*retrieved*	[43]
Onc	*patient-specific*	titanium[#]	Hemipelvic prostheses	14	60	[88]
Non-onc	*off-the-shelf*	Ti6Al4V	Metaphyseal components or cones	22	14	[50]
Onc	*patient-specific*	Ti6Al4V	Tibial prostheses	4	21.25	[105]
Onc	*patient-specific*	titanium[#]	Ulnar prosthesis	1	36	[84]
Onc	*patient-specific*	Ti6Al4V	Hemipelvic, humeral, and scapular prostheses	6	30	[77]
Non-onc	*patient-specific*	Ti6Al4V	Ankle fusion plate	1	36	[116]
Non-onc	*off-the-shelf*	titanium alloy[#]	Acetabular cups	32	93.48	[46]
Onc	*patient-specific*	NR	Hemipubic prostheses	5	23.6	[96]
Onc	*patient-specific*	Ti6Al4V	Hemipelvic prostheses	10	12.3	[90]
Onc	*patient-specific*	Ti6Al4V	Metacarpal prostheses	3	30	[87]
Non-onc	*patient-specific*	titanium alloy[#]	Hemiscaphoid prosthesis	1	24	[52]
Non-onc	*patient-specific*	NR	Talar prosthesis	1	12	[110]
Onc	*patient-specific*	Ti6Al4V ELI	Talar prosthesis	1	24	[112]
Onc	*patient-specific*	Ti6Al4V	Hemipelvic prostheses	2	24 and 48	[97]
Non-onc	*patient-specific*	CoCr	Talar prostheses	2	16 and 36	[113]

Onc = oncological; Non-onc = Non-oncological (trauma, disease, or infection)
[#] = not specified; [†] = median; NR = not reported.

Table 2
Challenges/complications reported in the published literature.

Challenges/complications	Notes	Refs.
Wound dehiscence	Related to bulky implants or presence of sharp edges. Can be prevented by implant redesign, smooth/polished implant surface, pre-implantation soft tissue expansion	Hemipelvis [48] Mandible [65] Mandible [66] Pelvis, calcaneus [78] Pelvis, calcaneus [79] Pelvis [88] Talus [109]
Implantation site access	Obstruction due to anatomical structures, may be circumvented by use of specialised surgical equipment	Self-stabilising vertebral body [69]
Infections (with/without implant removal)	Can be avoided by incorporating antimicrobial strategies, e.g., antimicrobial coatings for controlled release	Hemipelvis [48] Knee cones and sleeves [50] Pelvis [77] Pelvis [78] Pelvis, sacrum [79] Pelvis [88] Hip [98]
Muscle/soft tissue attachment	Integrated design features that allow soft tissues to be surgically attached	Clavicle, scapula, pelvis [76] Proximal tibia [102] Talus [112] Calcaneus [114] Calcaneus [115]
Fretting wear/loosening	Can be prevented by using a wear resistant alloy (e.g., CoCr) or wear resistant coatings, implant redesign	Pubis [96]
Scar tissue contracture – implant displacement	Correction involves scar tissue removal, revision surgery, skin grafting	Fifth toe [107]
Implant displacement or subsidence	Related to incorrect implant positioning or mismatch between implant geometry and anatomy	Intervertebral bodies [73] Pelvis [97]
Limited range of motion	May be improved by anatomically-accurate implant design, use of guides for implant positioning	Glenoid, humerus [82] Ulna [84] Elbow [85] Pelvix [97] Knee [103] Talus [108] Talus [109] Calcaneus [114]
Delayed wound healing	Preoperative nutritional evaluation and correction of deficiencies	Clavicle, scapula, pelvis [76]

mation on peri-implant bone microarchitecture and bone quality. Therefore, the clinical success of most implant-based treatments is ascertained from survival data. In this regard, together with better reporting of the clinical challenges (Table 2), more evidence is needed on the clinical effectiveness and long-term success of EBM and other additive manufacturing techniques. As has been pointed out by others in the context of custom-made spinal implants [141], a higher level of evidence will be necessary for personalised implants, in general. Furthermore, not only is there inconsistent reporting of the material used, e.g., several studies only indicate 'titanium' while some provide no information whatsoever, there is a great lack of reporting of percentage porosity, pore size, pore geometry, strut geometry, and the overall stiffness. The percentage porosity and pore sizes most frequently reported in the literature are in the range of 60–80% and 330–700 µm, respectively. It remains unclear, however, how much porosity and what pore size is optimal for a given anatomical location and a given clinical application. The pore/strut geometry and the overall implant design can be optimised at multiple length scales, i.e., micro-to-macro, based on established principles of bone mechanobiology in order to achieve consistent mechanobiological properties and ideal surface properties to promote bone healing and osseointegration [142]. Bone ingrowth and bone remodelling have traditionally been modelled independently using various mathematical/computational approaches, however, multiscale modelling approaches can reveal more accurate information on the mechanoresponse of bone after implant placement [143].

In clinical use, EBM-manufactured devices (both *off-the-shelf* and *patient-specific* implants) have noteworthy merits in comparison to those obtained by conventional manufacturing methods that produce solid structures. For example, reduced overall bulk minimises the stiffness mismatch between the implant and bone, and therefore stress shielding [12], while the porous geometry allows for bone (and soft tissue) ingrowth, allowing for improved mechanical anchorage [144]. *Patient-specific* implants allow for a better fit of the prosthesis and potentially better function (such as extended range of motion) compared to *off-the-shelf* implants, as in the case of acetabular cups. For many applications, conventional or *off-the-shelf* solutions are not available, e.g., maxillofacial reconstructions, and therefore *patient-specific* implants are the only option. Where such novel strategies push the envelope of skeletal deformities that can be corrected, regulatory procedures and standardisation guidelines for additively manufactured implants tend to vary globally and continue to evolve. The Food and Drug Administration (FDA), for example, only provides clearance to individual devices for specific intended uses, but not to materials for unspecified intended uses. At the same time, devices containing new materials may obtain clearance under the provision that the new material is at least as safe and effective as in an equivalent legally marketed device and does not raise additional questions of safety or effectiveness [145].

There are several new materials under development for EBM focussing on biomedical applications. Notable examples include NiTi shape memory alloys [146,147], and titanium-based alloys contain-

ing Nb, Zr, Ta (also referred to as TNZT alloys, e.g., Ti–35Nb–7Zr–5Ta) [148]. However, these are in the very early stages of development, with little or no information on biocompatibility or osseointegration, leaving them far from preclinical and/or clinical implementation.

Going forward, a potential direction for further development is customised strut design (and pore architecture) taking into consideration not only the expected microarchitecture of the anatomical site (for a given application) but also factors specific to the patient, including mechanical loading conditions. Finally, progressing beyond the simplistic view of a dense 'cortical bone-mimicking' shell and a porous 'trabecular bone-mimicking' interior [73], bone must be viewed as a multi-scale, hierarchically organised system [149,150] that continuously and continually adapts in response to mechanical stimulation [151,152].

Declaration of Competing Interest

The authors declare that they have no known competing financial interests or personal relationships that could have appeared to influence the work reported in this paper.

Acknowledgments

Financial support from the Swedish Research Council (Grant No. 2020-04715), Vinnova (2019-02607), Svenska Sällskapet för Medicinsk Forskning (SSMF), the Swedish state under the agreement between the Swedish government and the county councils, the ALF agreement (ALFGBG-966054), Centre for Additive Manufacturing, Metal (CAM^2) supported by Vinnova, the IngaBritt and Arne Lundberg Foundation, the Hjalmar Svensson Foundation, the Adlerbertska Foundation, the Dr. Felix Neubergh Foundation, Promobilia, and the Materials Science Area of Advance at Chalmers and the Department of Biomaterials, University of Gothenburg is acknowledged. None had any role in collection, analysis, and interpretation of data, or preparation of the manuscript.

References

[1] H.F. Hildebrand, Biomaterials – a history of 7000 years, BioNanoMaterials 14 (3-4) (2013) 119–133.
[2] N.J. Eynon-Lewis, D. Ferry, M.F. Pearse, Themistocles Gluck: an unrecognised genius, BMJ 305 (6868) (1992) 1534–1536.
[3] T. Gluck, Report on the positive results obtained by the modern surgical experiment regarding the suture and replacement of defects of superior tissue, as well as the utilization of re-absorbable and living tamponade in surgery, Clin. Orthop. Relat. Res. 469 (6) (2011) 1528–1535 469.
[4] V. Mironov, T. Trusk, V. Kasyanov, S. Little, R. Swaja, R. Markwald, Biofabrication: a 21st century manufacturing paradigm, Biofabrication 1 (2) (2009) 022001.
[5] L.E. Murr, Open-cellular metal implant design and fabrication for biomechanical compatibility with bone using electron beam melting, J. Mech. Behav. Biomed. Mater. (2017) 164–177.
[6] F.A. Shah, M. Trobos, P. Thomsen, A. Palmquist, Commercially pure titanium (cp-Ti) versus titanium alloy (Ti6Al4V) materials as bone anchored implants — is one truly better than the other? Mater. Sci. Eng. C Mater. Biol. Appl. 62 (2016) 960–966.
[7] A. Palmquist, O.M. Omar, M. Esposito, J. Lausmaa, P. Thomsen, Titanium oral implants: surface characteristics, interface biology and clinical outcome, J. R. Soc. Interface 7 (5) (2010) 515–527.
[8] L.Le Guéhennec, A. Soueidan, P. Layrolle, Y. Amouriq, Surface treatments of titanium dental implants for rapid osseointegration, Dent. Mater. 23 (7) (2007) 844–854.
[9] K. Markatos, O.D. Savvidou, A. Foteinou, S. Kosmadaki, I. Trikoupis, S.D. Goumenos, P.J. Papagelopoulos, Hallmarks in the history and development of total hip arthroplasty, Surg. Innov. 27 (6) (2020) 691–694.
[10] I.D. Learmonth, C. Young, C. Rorabeck, The operation of the century: total hip replacement, Lancet 370 (9597) (2007) 1508–1519.
[11] J.T. Evans, J.P. Evans, R.W. Walker, A.W. Blom, M.R. Whitehouse, A. Sayers, How long does a hip replacement last? A systematic review and meta-analysis of case series and national registry reports with more than 15 years of follow-up, Lancet 393 (10172) (2019) 647–654.
[12] R. Huiskes, H. Weinans, B. van Rietbergen, The relationship between stress shielding and bone resorption around total hip stems and the effects of flexible materials, Clin. Orthop. Relat. Res. 274 (1992) 124–134.
[13] L.E. Murr, S.M. Gaytan, F. Medina, H. Lopez, E. Martinez, B.I. Machado, D.H. Hernandez, L. Martinez, M.I. Lopez, R.B. Wicker, J. Bracke, Next-generation biomedical implants using additive manufacturing of complex, cellular and functional mesh arrays, Philos. Trans. A Math. Phys. Eng. Sci. 368 (2010) (1917) 1999–2032.
[14] L.E. Murr, K.N. Amato, S.J. Li, Y.X. Tian, X.Y. Cheng, S.M. Gaytan, E. Martinez, P.W. Shindo, F. Medina, R.B. Wicker, Microstructure and mechanical properties of open-cellular biomaterials prototypes for total knee replacement implants fabricated by electron beam melting, J. Mech. Behav. Biomed. Mater. 4 (7) (2011) 1396–1411.
[15] T. DebRoy, H.L. Wei, J.S. Zuback, T. Mukherjee, J.W. Elmer, J.O. Milewski, A.M. Beese, A. Wilson-Heid, A. De, W. Zhang, Additive manufacturing of metallic components – process, structure and properties, Prog. Mater. Sci. 92 (2018) 112–224.
[16] P. Heinl, L. Müller, C. Körner, R.F. Singer, F.A. Müller, Cellular Ti–6Al–4V structures with interconnected macro porosity for bone implants fabricated by selective electron beam melting, Acta Biomater. 4 (5) (2008) 1536–1544.
[17] J.E. Biemond, G. Hannink, N. Verdonschot, P. Buma, Bone in growth potential of electron beam and selective laser melting produced trabecular-like implant surfaces with and without a biomimetic coating, J. Mater. Sci. Mater. Med. 24 (3) (2013) 745–753.
[18] V.V. Popov, G. Muller-Kamskii, A. Kovalevsky, G. Dzhenzhera, E. Strokin, A. Kolomiets, J. Ramon, Design and 3D-printing of titanium bone implants: brief review of approach and clinical cases, Biomed. Eng. Lett. 8 (4) (2018) 337–344.
[19] C. Körner, Additive manufacturing of metallic components by selective electron beam melting — a review, Int. Mater. Rev. 61 (5) (2016) 361–377.
[20] E. Hryha, D. Riabov, Metal powder production for additive manufacturing, in: F.G Caballero (Ed.), Encyclopedia of Materials: Metals and Alloys, Elsevier, Oxford, 2022, pp. 264–271.
[21] S. Vock, B. Klöden, A. Kirchner, T. Weißgärber, B. Kieback, Powders for powder bed fusion: a review, Prog. Addit. Manuf. 4 (4) (2019) 383–397.
[22] A. Strondl, O. Lyckfeldt, H. Brodin, U. Ackelid, Characterization and control of powder properties for additive manufacturing, JOM 67 (3) (2015) 549–554.
[23] X. Zhao, S. Li, M. Zhang, Y. Liu, T.B. Sercombe, S. Wang, Y. Hao, R. Yang, L.E. Murr, Comparison of the microstructures and mechanical properties of Ti–6Al–4V fabricated by selective laser melting and electron beam melting, Mater. Des. 95 (2016) 21–31.
[24] Z.C. Cordero, H.M. Meyer, P. Nandwana, R.R. Dehoff, Powder bed charging during electron-beam additive manufacturing, Acta Mater. 124 (2017) 437–445.
[25] B. Vayre, F. Vignat, F. Villeneuve, Metallic additive manufacturing: state-of-the-art review and prospects, Mech. Ind. 13 (2) (2012) 89–96.
[26] C.J. Smith, S. Tammas-Williams, E. Hernandez-Nava, I. Todd, Tailoring the thermal conductivity of the powder bed in Electron Beam Melting (EBM) additive manufacturing, Sci. Rep. 7 (1) (2017) 10514.
[27] M. Kahlin, H. Ansell, J.J. Moverare, Fatigue behaviour of additive manufactured Ti6Al4V, with as-built surfaces, exposed to variable amplitude loading, Int. J. Fatigue 103 (2017) 353–362.
[28] S. Tammas-Williams, P.J. Withers, I. Todd, P.B. Prangnell, The effectiveness of hot isostatic pressing for closing porosity in titanium parts manufactured by selective electron beam melting, Metall. Mater. Trans. A 47 (5) (2016) 1939–1946.
[29] A. Abu-Issa, M. Lopez, C. Pickett, A. Escarcega, E. Arrieta, L.E. Murr, R.B. Wicker, M. Ahlfors, D. Godfrey, F. Medina, Effects of altered hot isostatic pressing treatments on the microstructures and mechanical performance of electron beam melted Ti-6Al-4V, J. Mater. Res. Technol. 9 (4) (2020) 8735–8743.
[30] X. Shui, K. Yamanaka, M. Mori, Y. Nagata, K. Kurita, A. Chiba, Effects of post-processing on cyclic fatigue response of a titanium alloy additively manufactured by electron beam melting, Mater. Sci. Eng. A Struct. Mater. 680 (2017) 239–248.
[31] M. Kahlin, H. Ansell, D. Basu, A. Kerwin, L. Newton, B. Smith, J.J. Moverare, Improved fatigue strength of additively manufactured Ti6Al4V by surface post processing, Int. J. Fatigue 134 (2020) 105497.
[32] D. Thomas, S.W. Gilbert, Costs and Cost Effectiveness of Additive Manufacturing, Special Publication (NIST SP), 1176, National Institute of Standards and Technology, Gaithersburg, MD, 2014 Accessed May 152022, doi:10.6028/NIST.SP.1176.
[33] P. Thomsen, J. Malmström, L. Emanuelsson, M. René, A. Snis, Electron beam-melted, free-form-fabricated titanium alloy implants: material surface characterization and early bone response in rabbits, J. Biomed. Mater. Res. B Appl. Biomater. 90 (1) (2009) 35–44.
[34] A. Palmquist, A. Snis, L. Emanuelsson, M. Browne, P. Thomsen, Long-term biocompatibility and osseointegration of electron beam melted, free-form-fabricated solid and porous titanium alloy: experimental studies in sheep, J. Biomater. Appl. 27 (8) (2013) 1003–1016.
[35] S. Ponader, C. von Wilmowsky, M. Widenmayer, R. Lutz, P. Heinl, C. Körner, R.F. Singer, E. Nkenke, F.W. Neukam, K.A. Schlegel, *In vivo* performance of selective electron beam-melted Ti-6Al-4V structures, J. Biomed. Mater. Res. A 92 (1) (2010) 56–62.
[36] N. Bertollo, R. Da Assuncao, N.J. Hancock, A. Lau, W.R. Walsh, Influence of electron beam melting manufactured implants on ingrowth and shear strength in an ovine model, J. Arthroplasty 27 (8) (2012) 1429–1436.
[37] G.M. de Peppo, A. Palmquist, P. Borchardt, M. Lennerås, J. Hyllner, A. Snis, J. Lausmaa, P. Thomsen, C. Karlsson, Free-form-fabricated commercially pure Ti and Ti6Al4V porous scaffolds support the growth of human embry-

onic stem cell-derived mesodermal progenitors, ScientificWorldJournal 2012 (2012) 646417.
[38] F.A. Shah, O. Omar, F. Suska, A. Snis, A. Matic, L. Emanuelsson, B. Norlindh, J. Lausmaa, P. Thomsen, A. Palmquist, Long-term osseointegration of 3D printed CoCr constructs with an interconnected open-pore architecture prepared by electron beam melting, Acta Biomater. 36 (2016) 296–309.
[39] F.A. Shah, E. Jergéus, A. Chiba, A. Palmquist, Osseointegration of 3D printed microalloyed CoCr implants—addition of 0.04% Zr to CoCr does not alter bone material properties, J. Biomed. Mater. Res. A 106 (6) (2018) 1655–1663.
[40] J.A. Tamayo, M. Riascos, C.A. Vargas, L.M. Baena, Additive manufacturing of Ti6Al4V alloy via electron beam melting for the development of implants for the biomedical industry, Heliyon 7 (5) (2021) e06892.
[41] R. Trisciuzzi, L. Fracassi, H.A. Martin, D. Monopoli Forleo, D. Amat, L. Santos-Ruiz, E. De Palma, A.M. Crovace, 41 Cases of treatment of cranial cruciate ligament rupture with porous TTA: three years of follow up, Vet. Sci. 6 (1) (2019) 18.
[42] L. Dall'Ava, H. Hothi, J. Henckel, A. Di Laura, P. Shearing, A. Hart, Characterization of dimensional, morphological and morphometric features of retrieved 3D-printed acetabular cups for hip arthroplasty, J. Orthop. Surg. Res. 15 (1) (2020) 157.
[43] L. Dall'Ava, H. Hothi, J. Henckel, A. Di Laura, R. Tirabosco, A. Eskelinen, J. Skinner, A. Hart, Osseointegration of retrieved 3D-printed, off-the-shelf acetabular implants, Bone Jt. Res. 10 (7) (2021) 388–400.
[44] F. Castagnini, B. Bordini, S. Stea, P.P. Calderoni, C. Masetti, L. Busanelli, Highly porous titanium cup in cementless total hip arthroplasty: registry results at eight years, Acta Orthop. Belg. 43 (8) (2019) 1815–1821.
[45] X. Geng, Y. Li, F. Li, X. Wang, K. Zhang, Z. Liu, H. Tian, A new 3D printing porous trabecular titanium metal acetabular cup for primary total hip arthroplasty: a minimum 2-year follow-up of 92 consecutive patients, J. Orthop. Surg. Res. 15 (1) (2020) 383.
[46] Y. Huang, Y.X. Zhou, H. Tian, J.W. Wang, W.G. Liu, H. Li, Minimum 7-year follow-up of a porous coated trabecular titanium cup manufactured with electron beam melting technique in primary total hip arthroplasty, Orthop. Surg. 13 (3) (2021) 817–824.
[47] H. Liang, T. Ji, Y. Zhang, Y. Wang, W. Guo, Reconstruction with 3D-printed pelvic endoprostheses after resection of a pelvic tumour, Bone Jt. J. 99-b (2) (2017) 267–275.
[48] T. Ji, Y. Yang, X. Tang, H. Liang, T. Yan, R. Yang, W. Guo, 3D-printed modular hemipelvic endoprosthetic reconstruction following periacetabular tumor resection: early results of 80 consecutive cases, J. Bone. Jt. Surg. Am. 102 (17) (2020) 1530–1541.
[49] Y. Zhang, L. Zhang, R. Sun, Y. Jia, X. Chen, Y. Liu, H. Oyang, L. Feng, A new 3D printed titanium metal trabecular bone reconstruction system for early osteonecrosis of the femoral head, Medicine 97 (26) (2018) e11088 (Baltimore).
[50] T. England, J. Pagkalos, L. Jeys, R. Botchu, R.C. Smith, Additive manufacturing of porous titanium metaphyseal components: early osseointegration and implant stability in revision knee arthroplasty, J. Clin. Orthop. Trauma 15 (2021) 60–64.
[51] S. Alshryda, A. Shah, S. Odak, J. Al-Shryda, B. Ilango, S.R. Murali, Acute fractures of the scaphoid bone: systematic review and meta-analysis, Surgeon 10 (4) (2012) 218–229.
[52] M.I. Rossello, Short-term findings of a custom-made 3D-printed titanium partial scaphoid prosthesis and scapholunate interosseous ligament reconstruction, BMJ Case Rep. 14 (7) (2021) e241090.
[53] M.I. Rossello, A case of total scaphoid titanium custom-made 3D-printed prostheses with one-year follow-up, Case Rep. Plast. Surg. Hand Surg. 7 (1) (2020) 7–12.
[54] H.R. Cho, T.S. Roh, K.W. Shim, Y.O. Kim, D.H. Lew, I.S. Yun, Skull reconstruction with custom made three-dimensional titanium implant, Arch. Craniofac. Surg. 16 (1) (2015) 11–16.
[55] E.K. Park, J.Y. Lim, I.S. Yun, J.S. Kim, S.H. Woo, D.S. Kim, K.W. Shim, Cranioplasty enhanced by three-dimensional printing: custom-made three-dimensional-printed titanium implants for skull defects, J. Craniofac. Surg. 27 (4) (2016) 943–949.
[56] N. Francaviglia, R. Maugeri, A. Odierna Contino, F. Meli, V. Fiorenza, G. Costantino, R.G. Giammalva, D.G. Iacopino, Skull bone defects reconstruction with custom-made titanium graft shaped with electron beam melting technology: preliminary experience in a series of ten patients, Acta Neurochir. Suppl. 124 (2017) 137–141.
[57] D. Policicchio, G. Casu, G. Dipellegrini, A. Doda, G. Muggianu, R. Boccaletti, Comparison of two different titanium cranioplasty methods: custom-made titanium prostheses versus precurved titanium mesh, Surg. Neurol. Int. 11 (2020) 148.
[58] J.Y. Kim, B.K. Jung, Y.S. Kim, T.S. Roh, I.S. Yun, Forehead reconstruction with a custom-made three-dimensional titanium implant in a Parry-Romberg syndrome patient, Arch. Craniofac. Surg. 19 (2) (2018) 135–138.
[59] P. Dérand, L.E. Rännar, J.M. Hirsch, Imaging, virtual planning, design, and production of patient-specific implants and clinical validation in craniomaxillofacial surgery, Craniomaxillofac. Trauma Reconstr. 5 (3) (2012) 137–144.
[60] B.A. Jereczek-Fossa, R. Orecchia, Radiotherapy-induced mandibular bone complications, Cancer Treat. Rev. 28 (1) (2002) 65–74.
[61] A. Thor, A. Palmquist, J.M. Hirsch, L.E. Rannar, P. Dérand, O. Omar, Clinical, morphological, and molecular evaluations of bone regeneration with an additive manufactured osteosynthesis plate, J. Craniofac. Surg. 27 (7) (2016) 1899–1904.
[62] F. Suska, G. Kjeller, P. Tarnow, E. Hryha, L. Nyborg, A. Snis, A. Palmquist, Electron beam melting manufacturing technology for individually manufactured jaw prosthesis: a case report, J. Oral Maxillofac. Surg. 74 (8) (2016) 1706.e1–1706.e15.
[63] Y.W. Lee, H.J. You, J.A. Jung, D.W. Kim, Mandibular reconstruction using customized three-dimensional titanium implant, Arch. Craniofac. Surg. 19 (2) (2018) 152–156.
[64] Y. Xia, Z.C. Feng, C. Li, H. Wu, C. Tang, L. Wang, H. Li, Application of additive manufacturing in customized titanium mandibular implants for patients with oral tumors, Oncol. Lett. 20 (4) (2020) 51.
[65] M. Mounir, A. Abou-ElFetouh, W. ElBeialy, R. Mounir, Patient-specific alloplastic endoprosthesis for reconstruction of the mandible following segmental resection: a case series, Cranio-Maxillo-Facial Surg. 48 (8) (2020) 719–723.
[66] M. Farid Shehab, N.M.A. Hamid, N.A. Askar, A.M. Elmardenly, Immediate mandibular reconstruction via patient-specific titanium mesh tray using electron beam melting/CAD/rapid prototyping techniques: one-year follow-up, Int. J. Med. Robot. 14 (3) (2018) e1895.
[67] U.L. Lee, J.S. Kwon, S.H. Woo, Y.J. Choi, Simultaneous bimaxillary surgery and mandibular reconstruction with a 3-dimensional printed titanium implant fabricated by electron beam melting: a preliminary mechanical testing of the printed mandible, J. Oral Maxillofac. Surg. 74 (7) (2016) 1501.e1–1501.e15.
[68] J.S. Zheng, X.H. Liu, X.Z. Chen, W.B. Jiang, A. Abdelrehem, S.Y. Zhang, M.J. Chen, C. Yang, Customized skull base-temporomandibular joint combined prosthesis with 3D-printing fabrication for craniomaxillofacial reconstruction: a preliminary study, Int. J. Oral Maxillofac. Surg. 48 (11) (2019) 1440–1447.
[69] N. Xu, F. Wei, X. Liu, L. Jiang, H. Cai, Z. Li, M. Yu, F. Wu, Z. Liu, Reconstruction of the upper cervical spine using a personalized 3D-printed vertebral body in an adolescent with Ewing sarcoma, Spine 41 (1) (2016) E50–E54.
[70] X. Li, Y. Wang, Y. Zhao, J. Liu, S. Xiao, K. Mao, Multilevel 3D printing implant for reconstructing cervical spine with metastatic papillary thyroid carcinoma, Spine 42 (22) (2017) E1326–e1330.
[71] F. Wei, Z. Li, Z. Liu, X. Liu, L. Jiang, M. Yu, N. Xu, F. Wu, L. Dang, H. Zhou, Z. Li, H. Cai, Upper cervical spine reconstruction using customized 3D-printed vertebral body in 9 patients with primary tumors involving C2, Ann. Transl. Med. 8 (6) (2020) 332.
[72] K. Phan, A. Sgro, M.M. Maharaj, P. D'Urso, R.J. Mobbs, Application of a 3D custom printed patient specific spinal implant for C1/2 arthrodesis, J. Spine Surg. 2 (4) (2016) 314–318.
[73] M. Girolami, S. Boriani, S. Bandiera, G. Barbanti-Bródano, R. Ghermandi, S. Terzi, G. Tedesco, G. Evangelisti, V. Pipola, A. Gasbarrini, Biomimetic 3D-printed custom-made prosthesis for anterior column reconstruction in the thoracolumbar spine: a tailored option following en bloc resection for spinal tumors: preliminary results on a case-series of 13 patients, Eur. Spine J. 27 (12) (2018) 3073–3083.
[74] R.J. Mobbs, M. Coughlan, R. Thompson, C.E. Sutterlin, K. Phan, The utility of 3D printing for surgical planning and patient-specific implant design for complex spinal pathologies: case report, J. Neurosurg. Spine 26 (4) (2017) 513–518.
[75] T.L. Siu, J.M. Rogers, K. Lin, R. Thompson, M. Owbridge, Custom-made titanium 3-dimensional printed interbody cages for treatment of osteoporotic fracture–related spinal deformity, World Neurosurg. 111 (2018) 1–5.
[76] H. Fan, J. Fu, X. Li, Y. Pei, X. Li, G. Pei, Z. Guo, Implantation of customized 3-D printed titanium prosthesis in limb salvage surgery: a case series and review of the literature, World J. Surg. Oncol. 13 (2015) 308.
[77] G. Beltrami, G. Ristori, A. Galeotti, G. Scoccianti, A. Tamburini, D. Campanacci, R. Capanna, M. Innocenti, A hollow, custom-made prosthesis combined with a vascularized flap and bone graft for skeletal reconstruction after bone tumour resection, Surg. Oncol. 36 (2021) 56–60.
[78] A. Angelini, G. Trovarelli, A. Berizzi, E. Pala, A. Breda, P. Ruggieri, Three--dimension-printed custom-made prosthetic reconstructions: from revision surgery to oncologic reconstructions, Int. Orthop. 43 (1) (2019) 123–132.
[79] A. Angelini, D. Kotrych, G. Trovarelli, A. Szafrański, A. Bohatyrewicz, P. Ruggieri, Analysis of principles inspiring design of three-dimensional-printed custom-made prostheses in two referral centres, Int. Orthop. 44 (5) (2020) 829–837.
[80] J.L. Aranda, M.F. Jiménez, M. Rodríguez, G. Varela, Tridimensional titanium-printed custom-made prosthesis for sternocostal reconstruction, Eur. J. Cardio Thorac. Surg. 48 (4) (2015) e92–e94 official journal of the European Association for Cardio-thoracic Surgery.
[81] Y. Zou, Y. Yang, Q. Han, K. Yang, K. Zhang, J. Wang, Y. Zou, Novel exploration of customized 3D printed shoulder prosthesis in revision of total shoulder arthroplasty: a case report, Medicine 97 (47) (2018) e13282 (Baltimore).
[82] H. Hu, W. Liu, Q. Zeng, S. Wang, Z. Zhang, J. Liu, Y. Zhang, Z. Shao, B. Wang, The personalized shoulder reconstruction assisted by 3D printing technology after resection of the proximal humerus tumours, Cancer Manag. Res. 11 (2019) 10665–10673.
[83] J.W. Park, H.G. Kang, J.H. Kim, H.S. Kim, New 3-dimensional implant application as an alternative to allograft in limb salvage surgery: a technical note on 10 cases, Acta Orthop. 91 (4) (2020) 489–496.
[84] A.S.E. Brandsma, E.J.D. Veen, A.W.J.M. Glaudemans, P.C. Jutte, J.J.W. Ploegmakers, Customized treatment for an oncologic lesion near a joint: case report of a custom-made 3D-printed prosthesis for a grade II chondrosarcoma of the proximal ulna, J. Tissue Eng. Regen. Med. 5 (1) (2020) 42–45.
[85] N. Wu, S. Li, Y. Liu, A. Zhang, B. Chen, Q. Han, J. Wang, Novel exploration of 3D printed personalized total elbow arthroplasty to solve the severe bone

defect after internal fixation failure of comminuted distal humerus fracture: a case report, Medicine 99 (31) (2020) e21481 (Baltimore).-e21481.
[86] G. Beltrami, Custom 3D-printed finger proximal phalanx as salvage of limb function after aggressive recurrence of giant cell tumour, BMJ Case Rep. 2018 (2018) bcr2018226007.
[87] L. Xu, H. Qin, Z. Cheng, W.B. Jiang, J. Tan, X. Luo, W. Huang, 3D-printed personalised prostheses for bone defect repair and reconstruction following resection of metacarpal giant cell tumours, Ann. Transl. Med. 9 (18) (2021) 1421.
[88] C. Zoccali, J. Baldi, D. Attala, A. Scotto di Uccio, L. Cannavò, G. Scotto, A. Luzzati, 3D-printed titanium custom-made prostheses in reconstruction after pelvic tumor resection: indications and results in a series of 14 patients at 42 months of average follow-up, J. Clin. Med. 10 (16) (2021).
[89] W. Peng, R. Zheng, H. Wang, X. Huang, Reconstruction of bony defects after tumor resection with 3D-printed anatomically conforming pelvic prostheses through a novel treatment strategy, Biomed. Res. Int. 2020 (2020) 8513070.
[90] L. Xu, H. Qin, J. Tan, Z. Cheng, X. Luo, H. Tan, W. Huang, Clinical study of 3D printed personalized prosthesis in the treatment of bone defect after pelvic tumor resection, J. Orthop. Transl. 29 (2021) 163–169.
[91] Q. Han, K. Zhang, Y. Zhang, C. Wang, K. Yang, Y. Zou, B. Chen, J. Wang, Individual resection and reconstruction of pelvic tumor with three-dimensional printed customized hemi-pelvic prosthesis: a case report, Medicine 98 (36) (2019) e16658 (Baltimore).-e16658.
[92] Y. Wang, W. Guo, D. Shen, X. Tang, Y. Yang, T. Ji, X. Xu, Surgical treatment of primary osteosarcoma of the sacrum: a case series of 26 patients, Spine 42 (16) (2017) 1207–1213.
[93] D. Kim, J.Y. Lim, K.W. Shim, J.W. Han, S. Yi, D.H. Yoon, K.N. Kim, Y. Ha, G.Y. Ji, D.A. Shin, Sacral reconstruction with a 3D-printed implant after hemisacrectomy in a patient with sacral osteosarcoma: 1-year follow-up result, Yonsei Med. J. 58 (2) (2017) 453–457.
[94] J. Wang, L. Min, M. Lu, Y. Zhang, Y. Wang, Y. Luo, Y. Zhou, H. Duan, C. Tu, Three-dimensional-printed custom-made hemipelvic endoprosthesis for primary malignancies involving acetabulum: the design solution and surgical techniques, J. Orthop. Surg. Res. 14 (1) (2019) 389.
[95] Y. Zhang, L. Min, M. Lu, J. Wang, Y. Wang, Y. Luo, Y. Zhou, H. Duan, C. Tu, Three-dimensional-printed customized prosthesis for pubic defect: prosthesis design and surgical techniques, J. Orthop. Surg. Res. 15 (1) (2020) 261.
[96] Y. Zhang, L. Min, M. Lu, J. Wang, Y. Wang, Y. Luo, Y. Zhou, H. Duan, C. Tu, Three-dimensional-printed customized prosthesis for pubic defect: clinical outcomes in 5 cases at a mean follow-up of 24 months, BMC Musculoskel. Disord. 22 (1) (2021) 405.
[97] D. Zhu, J. Fu, L. Wang, Z. Guo, Z. Wang, H. Fan, Reconstruction with customized, 3D-printed prosthesis after resection of periacetabular Ewing's sarcoma in children using "triradiate cartilage-based" surgical strategy: a technical note, J. Orthop. Transl. 28 (2021) 108–117.
[98] G. Burastero, L. Cavagnaro, F. Chiarlone, A. Zanirato, L. Mosconi, L. Felli, F.D.R. de Lorenzo, Clinical study of outcomes after revision surgery using porous titanium custom-made implants for severe acetabular septic bone defects, Int. Orthop. 44 (10) (2020) 1957–1964.
[99] M. Durand-Hill, J. Henckel, A. Di Laura, A.J. Hart, Can custom 3D printed implants successfully reconstruct massive acetabular defects? A 3D-CT assessment, J. Orthop. Res. 38 (12) (2020) 2640–2648.
[100] H. Zhang, Y. Liu, Q. Dong, J. Guan, J. Zhou, Novel 3D printed integral customized acetabular prosthesis for anatomical rotation center restoration in hip arthroplasty for developmental dysplasia of the hip Crowe type III: a case report, Medicine 99 (40) (2020) e22578 (Baltimore).-e22578.
[101] G. Hou, B. Liu, Y. Tian, Z. Liu, F. Zhou, H. Ji, Z. Zhang, Y. Guo, Y. Lv, Z. Yang, P. Wen, Y. Zheng, Y. Cheng, An innovative strategy to treat large metaphyseal segmental femoral bone defect using customized design and 3D printed micro-porous prosthesis: a prospective clinical study, J. Mater. Sci. Mater. Med. 31 (8) (2020) 66.
[102] W. Luo, L. Huang, H. Liu, W. Qu, X. Zhao, C. Wang, C. Li, T. Yu, Q. Han, J. Wang, Y. Qin, Customized knee prosthesis in treatment of giant cell tumors of the proximal tibia: application of 3-dimensional printing technology in surgical design, Med. Sci. Monit. 23 (2017) 1691–1700.
[103] W. Liu, Z. Shao, S. Rai, B. Hu, Q. Wu, H. Hu, S. Zhang, B. Wang, Three-dimensional-printed intercalary prosthesis for the reconstruction of large bone defect after joint-preserving tumor resection, J. Surg. Oncol. 121 (3) (2020) 570–577.
[104] M. Lu, J. Wang, F. Tang, L. Min, Y. Zhou, W. Zhang, C. Tu, A three-dimensional printed porous implant combined with bone grafting following curettage of a subchondral giant cell tumour of the proximal tibia: a case report, BMC Surg. 19 (1) (2019) 29.
[105] W.K. Guder, J. Hardes, M. Nottrott, L.E. Podleska, A. Streitburger, Highly Cancellous titanium alloy (TiAl6V4) surfaces on three-dimensionally printed, custom-made intercalary tibia prostheses: promising short- to intermediate-term results, J. Pers. Med. 11 (5) (2021) 351.
[106] M. Lu, Y. Li, Y. Luo, W. Zhang, Y. Zhou, C. Tu, Uncemented three-dimensional-printed prosthetic reconstruction for massive bone defects of the proximal tibia, World J. Surg. Oncol. 16 (1) (2018) 47 -47.
[107] C. Chandhanayingyong, K. Srikong, C. Puncreobutr, B. Lohwongwatana, R. Phimolsarnti, B. Chuckpaiwong, Three-dimensional printed, proximal phalangeal prosthesis with metatarsophalangeal joint arthroplasty for the treatment of a giant cell tumor of the fifth toe: the first case report, Int. J. Surg. Case Rep. 73 (2020) 84–89.
[108] R.J. Kadakia, C.C. Akoh, J. Chen, A. Sharma, S.G. Parekh, 3D printed total talus replacement for avascular necrosis of the talus, Foot Ankle Int. 41 (12) (2020) 1529–1536.
[109] D.J. Scott, J. Steele, A. Fletcher, S.G. Parekh, Early outcomes of 3D printed total talus arthroplasty, Foot Ankle Spec. 13 (5) (2020) 372–377.
[110] R.M. Hussain, Metallic 3D printed total talus replacement: a case study, J. Foot Ankle Surg. 60 (3) (2021) 634–641.
[111] J. Tracey, D. Arora, C.E. Gross, S.G. Parekh, Custom 3D-printed total talar prostheses restore normal joint anatomy throughout the hindfoot, Foot Ankle Spec. 12 (1) (2019) 39–48.
[112] J. Huang, F. Xie, X. Tan, W. Xing, Y. Zheng, C. Zeng, Treatment of osteosarcoma of the talus with a 3D-printed talar prosthesis, J. Foot Ankle Surg. 60 (1) (2021) 194–198.
[113] G. Strand, C. Juels, J. Nowak, Custom total talus replacement as a salvage option for failed total ankle arthroplasty: a prospective report of two cases, Foot Ankle Surg. (N Y) 2 (1) (2022) 100113.
[114] J. Imanishi, P.F.M. Choong, Three-dimensional printed calcaneal prosthesis following total calcanectomy, Int. J. Surg. Case Rep. 10 (2015) 83–87.
[115] J.W. Park, H.G. Kang, K.M. Lim, J.H. Kim, H.S. Kim, Three-dimensionally printed personalized implant design and reconstructive surgery for a bone tumor of the calcaneus: a case report, JBJS Case Connect. 8 (2) (2018) e25.
[116] Y. Yao, Z. Mo, G. Wu, J. Guo, J. Li, L. Wang, Y. Fan, A personalized 3D-printed plate for tibiotalocalcaneal arthrodesis: design, fabrication, biomechanical evaluation and postoperative assessment, Comput. Biol. Med. 133 (2021) 104368.
[117] F.A. Shah, P. Thomsen, A. Palmquist, Osseointegration and current interpretations of the bone-implant interface, Acta Biomater. 84 (2019) 1–15.
[118] F.A. Shah, Osteocytes as Indicators of Bone Quality - Multiscale Structure–Composition Characterisation of the Bone-Implant Interface, Göteborgs Universitet, Göteborg, 2017 PhD Thesis.
[119] R. Brånemark, A Biomechanical Study of Osseointegration, Göteborgs Universitet, Göteborg, 1996 PhD Thesis.
[120] M. Esposito, J.M. Hirsch, U. Lekholm, P. Thomsen, Biological factors contributing to failures of osseointegrated oral implants. (I). Success criteria and epidemiology, Eur. J. Oral Sci. 106 (1) (1998) 527–551.
[121] F.A. Shah, A. Snis, A. Matic, P. Thomsen, A. Palmquist, 3D printed Ti6Al4V implant surface promotes bone maturation and retains a higher density of less aged osteocytes at the bone-implant interface, Acta Biomater. 30 (2016) 357–367.
[122] P. Stenlund, S. Kurosu, Y. Koizumi, F. Suska, H. Matsumoto, A. Chiba, A. Palmquist, Osseointegration enhancement by Zr doping of Co-Cr-Mo implants fabricated by electron beam melting, Addit Manuf 6 (2015) 6–15.
[123] L. Chambrone, J. Mandia, J.A. Shibli, G.A. Romito, M. Abrahao, Dental implants installed in irradiated jaws: a systematic review, J. Dent. Res. 92 (12) (2013) 119s–130s Suppl.
[124] S. Ihde, S. Kopp, K. Gundlach, V.S. Konstantinović, Effects of radiation therapy on craniofacial and dental implants: a review of the literature, Oral Surg. Oral Med. Oral Pathol. Oral Radiol. Endod. 107 (1) (2009) 56–65.
[125] J. Nyberg, S. Hertzman, B. Svensson, C.B. Johansson, Osseointegration of implants in irradiated bone with and without hyperbaric oxygen treatment: an experimental study in rat Tibiae, Int. J. Oral Maxillofac. Implants 28 (3) (2013) 739–746.
[126] L.O. Ohrnell, R. Brånemark, J. Nyman, P. Nilsson, P. Thomsen, Effects of irradiation on the biomechanics of osseointegration. An experimental *in vivo* study in rats, Scand. J. Plast. Reconstr. Surg. Hand Surg. 31 (4) (1997) 281–293.
[127] G. Granström, Radiotherapy, osseointegration and hyperbaric oxygen therapy, Periodontology 33 (2003) (2000) 145–162.
[128] F. Jegoux, O. Malard, E. Goyenvalle, E. Aguado, G. Daculsi, Radiation effects on bone healing and reconstruction: interpretation of the literature, Oral Surg. Oral Med. Oral Pathol. Oral Radiol. Endod. 109 (2) (2010) 173–184.
[129] J.Y. Li, E.H. Pow, L.W. Zheng, L. Ma, D.L. Kwong, L.K. Cheung, Dose-dependent effect of radiation on titanium implants: a quantitative study in rabbits, Clin. Oral. Implants Res. 25 (2) (2014) 260–265.
[130] A.A. Johnsson, T. Sawaii, M. Jacobsson, G. Granström, I. Turesson, A histomorphometric and biomechanical study of the effect of delayed titanium implant placement in irradiated rabbit bone, Clin. Implant Dent. Relat. Res. 2 (1) (2000) 42–49.
[131] J. Wang, B. Zhou, X.S. Liu, A.J. Fields, A. Sanyal, X. Shi, M. Adams, T.M. Keaveny, X.E. Guo, Trabecular plates and rods determine elastic modulus and yield strength of human trabecular bone, Bone 72 (2015) 71–80.
[132] R.M. Zebaze, A. Ghasem-Zadeh, A. Bohte, S. Iuliano-Burns, M. Mirams, R.I. Price, E.J. Mackie, E. Seeman, Intracortical remodelling and porosity in the distal radius and post-mortem femurs of women: a cross-sectional study, Lancet 375 (9727) (2010) 1729–1736.
[133] R.P. van Hove, I.N. Sierevelt, B.J. van Royen, P.A. Nolte, Titanium-nitride coating of orthopaedic implants: a review of the literature, Biomed. Res. Int. 2015 (2015) 485975.
[134] L. Leyssens, B. Vinck, C. Van Der Straeten, F. Wuyts, L. Maes, Cobalt toxicity in humans-a review of the potential sources and systemic health effects, Toxicology 387 (2017) 43–56.
[135] P. Johansson, R. Jimbo, Y. Naito, P. Kjellin, F. Currie, A. Wennerberg, Polyether ether ketone implants achieve increased bone fusion when coated with nano-sized hydroxyapatite: a histomorphometric study in rabbit bone, Int. J. Nanomedicine 11 (2016) 1435–1442.

[136] R. Ma, Z. Yu, S. Tang, Y. Pan, J. Wei, T. Tang, Osseointegration of nanohydroxyapatite- or nano-calcium silicate-incorporated polyetheretherketone bioactive composites *in vivo*, Int. J. Nanomedicine 11 (2016) 6023–6033.
[137] G. Del Guercio, M. Galati, A. Saboori, Electron beam melting of Ti-6Al-4V lattice structures: correlation between post heat treatment and mechanical properties, Int. J. Adv. Manuf. Technol. 116 (11) (2021) 3535–3547.
[138] A. du Plessis, I. Yadroitsev, I. Yadroitsava, S.G. Le Roux, X-Ray microcomputed tomography in additive manufacturing: a review of the current technology and applications, 3D Print. Addit. Manuf. 5 (3) (2018) 227–247.
[139] J. Fieres, P. Schumann, C. Reinhart, Predicting failure in additively manufactured parts using X-ray computed tomography and simulation, Procedia Eng. 213 (2018) 69–78.
[140] E. Hong, D.S. Kwak, I.B. Kim, Morphological symmetry of the radius and ulna—can contralateral forearm bones utilize as a reliable template for the opposite side? PLoS One 16 (10) (2021) e0258232.
[141] W.J. Choy, R.J. Mobbs, Current state of 3D-printed custom-made spinal implants, Lancet Digit. Health 1 (4) (2019) e149–e150.
[142] C. Metz, G.N. Duda, S. Checa, Towards multi-dynamic mechano-biological optimization of 3D-printed scaffolds to foster bone regeneration, Acta Biomater. 101 (2020) 117–127.
[143] J.M. García-Aznar, G. Nasello, S. Hervas-Raluy, M.Á. Pérez, M.J. Gómez-Benito, Multiscale modeling of bone tissue mechanobiology, Bone 151 (2021) 116032.
[144] S. Cleemput, S.E.F. Huys, R. Cleymaet, W. Cools, M.Y. Mommaerts, Additively manufactured titanium scaffolds and osteointegration - meta-analyses and moderator-analyses of *in vivo* biomechanical testing, Biomater. Res. 25 (1) (2021) 18.
[145] M. Di Prima, J. Coburn, D. Hwang, J. Kelly, A. Khairuzzaman, L. Ricles, Additively manufactured medical products – the FDA perspective, 3D Print. Med. 2 (1) (2016) 1.
[146] C. Wang, X.P. Tan, Z. Du, S. Chandra, Z. Sun, C.W.J. Lim, S.B. Tor, C.S. Lim, C.H. Wong, Additive manufacturing of NiTi shape memory alloys using pre-mixed powders, J. Mater. Process. Technol. 271 (2019) 152–161.
[147] Q. Zhou, M.D. Hayat, G. Chen, S. Cai, X. Qu, H. Tang, P. Cao, Selective electron beam melting of NiTi: microstructure, phase transformation and mechanical properties, Mater. Sci. Eng. A 744 (2019) 290–298.
[148] K. Yang, J. Wang, H. Tang, Y. Li, Additive manufacturing of *in-situ* reinforced Ti–35Nb–5Ta–7Zr (TNTZ) alloy by selective electron beam melting (SEBM), J. Alloy. Compd. 826 (2020) 154178.
[149] M.D. McKee, D.J. Buss, N. Reznikov, Mineral tessellation in bone and the stenciling principle for extracellular matrix mineralization, J. Struct. Biol. 214 (1) (2022) 107823.
[150] D.J. Buss, R. Kröger, M.D. McKee, N. Reznikov, Hierarchical organization of bone in three dimensions: a twist of twists, J. Struct. Biol. X 6 (2022) 100057.
[151] A.G. Robling, C.H. Turner, Mechanical signaling for bone modeling and remodeling, Crit. Rev. Eukaryot. Gene Expr. 19 (4) (2009) 319–338.
[152] Z. Li, R. Müller, D. Ruffoni, Bone remodeling and mechanobiology around implants: insights from small animal imaging, J. Orthop. Res. 36 (2) (2018) 584–593.